Impact of pressure on optoelectronic and thermoelectric properties of vacancy-ordered double perovskite K_2SeCl_6

Roll: MS201301
Session: 2020-2021

Thesis submitted to the Department of Physics at
Jashore University of Science and Technology
in partial fulfillment of the requirements
for the degree of Masters of Science
in Physics

February, 2024

Abstract

In the field of optoelectronics and other sustainable energy conversion applications, vacancy-ordered double perovskite materials are thought to be the most promising resources nowadays. In this thesis we represent the structural, mechanical, electronic, optical and thermoelectric properties of vacancy-ordered double perovskite K_2SeCl_6 studied by first principle calculations under ambient and different hydrostatic pressure ranging upto 80 GPa. The structural stability of the compound is ensured by the Goldsmiths tolerance factor (0.98) and negative formation energy (-0.53 eV). It exhibits good mechanical stability when pressure is applied revealing that induced pressure has a substantial influence on the mechanical stability. The bandstructure shows p-type semiconducting nature with an indirect band gap of 2.502 eV at ambient condition and band gap decreases gradually with induced pressure. The optical absorbance and conductivity increases with increasing pressure making them more appropriate for optoelectronic applications in Ultra-violet region. The optical analysis has been conducted by computing the dielectric function, absorption coefficient, conductivity, optical reflection, and refractive index. Thermoelectric charecteristics are investigated using BoltzTraP to estimate the electrical and tharmal conductivities, seebeck coefficient, power factor and figure of merit. The computed value of figure of merit at room temperature (0.78) reveals the promising potential for renewable energy applications of K_2SeCl_6 in both ambient and pressurized conditions.

Acknowledgements

Firstly, I praise and thank almighty Allah, the Lord of the worlds, the Most Merciful, the Guider of hearts, the Provider of sustenance, the Owner of life and death. I would like to thank my supervisor Dr. Mohammad Abdur Rashid, for his constant support and guidance to complete my thesis properly. During the period of this thesis, he always shows me confidence which is really invaluable. Also, my gratitude goes to all the faculty members of the Department of Physics for many helpful discussion at different times. I wish to extend my profound gratitude and appreciation to the Quantum Materials Simulation Lab (QMSL) for its resources throughout the course of my research. Working in the lab has been an enriching and enlightening experience for me. I am deeply thankful to all the members of the research lab for their guidance, assistance and willingness to share knowledge which has been invaluable for the quality of my research. I appreciate the efforts to maintain a well-organized and well-stocked environment of the lab. On a personal note, I would like to thank my parents for their sacrifice and support over the years. Their love and encouragement always give me mental support to continue my study smoothly.

Contents

List of Figures

LIST OF FIGURES

List of Tables

Impact of pressure on optoelectronic and thermoelectric properties of vacancy-ordered double perovskite K_2SeCl_6

Chapter 1

Introduction

Vacancy-ordered double perovskite materials represent a fascinating class of crystalline compounds that have gained significant attention in the field of materials science and condensed matter physics [1, 2]. These materials are known for their unique structural and electronic properties, which make them promising candidates for a wide range of applications, including in the fields of electronics, magnetism, and energy conversion [3, 4]. To understand what makes vacancy-ordered double perovskites special, it's essential to break down their name. "Double perovskite" refers to a particular crystal structure characterized by the general formula $A_2BB'X_6$, where A stands for an alkali earth metals, B, B′ are two different transition metals and X represents an anion [5]. These B, B′ sites can be occupied by different transition metals, creating a wide range of possibilities for tailoring their properties [6, 7]. In case of vacancy-ordered double perovskites, there is a controlled distribution of vacant atomic sites within the structure, which can lead to remarkable effects on the physical properties [8, 9]. The ordering of these vacancies can be seen as a kind of atomic chessboard where specific atoms are deliberately missing, creating a complex and intriguing arrangement [10, 11]. Vacancy-ordered double perovskites have recently garnered attention due to their tunable electronic properties, making them versatile materials for applications such as solid oxide fuel cells, thermoelectric and

optoelectronic devices [12,13]. The presence of vacancies in the crystal lattice enables control over electronic behavior, leading to materials with diverse electrical conductivity, from metals to semiconductors [14–16]. Additionally, the ionic conductivity of these materials is enhanced, making them promising for use in electrochemical devices [17–19]. Researchers are exploring their potential in energy conversion, storage, and as efficient materials for thermoelectric applications, leveraging the unique properties arising from vacancy ordering in the perovskite structure [20–24].

In recent years, researchers are studing vacancy-ordered double perovskite materials enormously. As example, Aiyeshah Alhodaib et al. studied the vacancy-ordered double perovskites In_2PtX_6 (X = Cl, Br, I) for solar cells and renewable energy applications as an alternative of hybrid perovskites [25]. Fei Zhang et al. and Zhipeng Chen et al. explored the highly stable vacancy-ordered double perovskite Rb_2ZrCl_6 with broadband emission for down-conversion white light-emitting diodes [26]. Faizan et al. and Muhammad et al. studied the electronic and optical properties of vacancy-ordered double perovskites A_2BX_6 (A = Rb, Cs; B = Sn, Pd, Pt and X = Cl, Br, I) and showed them to be the suitable candidate for high performance single and multi junction perovskite solar cells [27]. Cucco et al. and Bouder et al. reported Cs_2TiX_6 and Cs_2ZrX_6 (X = Br, I) vacancy-ordered double perovskites as a stable absorber with interesting electronic and optical properties, such as a bandgap in the visible, and long carrier diffusion lengths [28]. Bhumla et al. and Preeti et al. studied the vacancy-ordered double perovskites Cs_2BI_6 (B = Pt, Pd, Te, Sn) in search of promising renewable energy conversion applications [29]. One of the most well-known examples of a vacancy-ordered double perovskite is K_2SeCl_6 (potassium selenochlorate). In which, the potassium (K) and selenium (Se) atoms are arranged in an ordered fashion within the crystal lattice, with specific vacancies that result in a unique electronic and magnetic structure [30]. This unique arrangement offers exciting prospects for exploring the inherent properties of the material and manipulating its characteristics through appropriate modifications. The presence of Se(IV) in K_2SeCl_6 makes it intriguing for studying the electronic structure and chemical behavior of selenium in this unique oxidation state [31]. Investigation of K_2SeCl_6 both in pressurized and ambient condition can contribute to our fun-

damental understanding of materials in chemistry, crystallography, and solid-state physics.

The pressure effect on vacancy-ordered double perovskite materials is a fascinating area of research that sheds light on the dynamic relationship between external pressure and the structural, electronic, and magnetic properties of these compounds [32, 33]. Pressure, or hydrostatic compression, has been shown to induce significant changes in the physical properties of vacancy-ordered double perovskite materials, offering new avenues for tuning and controlling their behavior [34, 35]. Pressure can induce structural phase transitions in materials [36]. At high pressures, the atomic arrangement within the crystal lattice can undergo significant alterations [37]. This can lead to changes in bond lengths, bond angles, and the overall symmetry of the crystal structure. Changes in the crystal structure under pressure can result in modifications of the electronic and magnetic properties [38,39]. For example, pressure may affect the density of states near the Fermi level, leading to alterations in electrical conductivity or electronic bandgaps [40]. Pressure can also influence the magnetic ordering and magnetic moments of the atoms within the material [41, 42].

In this thesis, we investigate the changes in mechanical, optoelectronic, and thermoelectric porperties of K_2SeCl_6 by subjecting it to varying pressure conditions upto 80 GPa. We follow the first-principle calculation method using Density Functional Theory (DFT) [43,44] as implemented in WIEN2k [45,46] code. DFT is a computational method used in quantum mechanics to describe the electronic structure and properties of solids. It provides a powerful approach for studying the behavior of electrons within a material. At its core, DFT is based on the idea that the total energy of a system can be expressed in terms of the electronic density rather than the complex wave functions of individual electrons [47]. By solving the underlying mathematical equations, it provides insights into the behavior of electrons and their interactions, allowing scientists to predict and understand various properties and phenomena [48]. WIEN2k is a versatile and sophisticated software package for electronic structure calculations in materials science. It provides a comprehensive set

of tools for simulating and analyzing the electronic properties of solids [49]. It employs the full-potential linearized augmented plane wave (FP-LAPW) method [50], which allows an accurate calculations of electronic structures and related properties. WIEN2k incorporates several advanced features, including spin-orbit coupling, the treatment of disordered systems, and the calculation of optical and magnetic properties. It can handle a wide range of crystal structures and is particularly useful for investigating complex and challenging materials. BoltzTraP [51] is employed to investigate the electronic transport properties and explore possible thermoelectric uses. We choose to investigate our system with both ambient and under externally applied hydrostatic pressure because material behaviour changes on application of a strain, or to model interactions between a substrate and molecule.

This thesis aims to provide a comprehensive understanding of the structural, mechanical, electronic, optical, and thermoelectric properties of K_2SeCl_6 under ambient and applied hydrostatic pressure. In Chapter 2, we discuss the basic quantum mechanics as the base of density functional theory. Starting from Schrödinger equation we dispute the criteria for the ground state wave function. We shortly discuss the Born oppenheimar approximation and the Hartree-Fock approach with its limitations in this chapter. In chapter 3 we discuss the theoritical density functional theory. Starting with the Thomas Fermi model we discuss the Hohenberg Khon theorems, Kohn Sham equation with the equivalent flowchart and the exchange correletion functionals that can be used to solve a many body system. In chapter 4 we weigh up the structural, electronic, optical and thermoelectric properties of K_2SeCl_6 vacancy-ordered perovskite material under ambient conditions. With applied pressure upto 80 GPa, we represent the possible changes in inherent properties of K_2SeCl_6 in chapter 5. In last chapter we make a conclusion about the properties that are changes because of induced pressure, and possible potential applications of the material under both ambient and pressurized conditions.

Chapter 2

Basic Quantum Mechanics

Density functional theory (DFT) is built upon the foundation of basic quantum mechanics, particularly the Schrödinger equation. The Schrödinger equation deals with all issues in the electrical structure of matter However, in most circumstances, one is only concerned with atoms and molecules that do not have time-dependent interactions. So, we may concentrate on the Schrödinger equation that is time independent. This is supplied by the Born-Oppenheimer non relativistic approximation for an isolated N electron atomic or molecular system [52].

$$\hat{H}\Psi = E\Psi \tag{2.1}$$

Here, $\hat{H}$ is the Hamiltonian operator, Ψ represents the wave function, and E corresponds to the energy of the system. Equation 2.1 must be solved while taking into account the proper boundary conditions. For an atom or molecule or with the proper periodic boundary conditions for a regular finite solid, Ψ must behave well everywhere and in particular decay to zero at infinity. We are aware that the first and foremost postulate of fundamental quantum mechanics is that "a particle's state is completely described by its time independent wave function," meaning that the wave function contains all the information required to understand a particle's state. Quantum mechanically it is denoted by Ψ. In essence, it has no physical

significance. The square of it's modulas gives the probability of finding a particle in a given region. $|\Psi|^2$ is the probability distribution function in the sence that

$$|\Psi(r^N, s^N)|^2 \; dr^N = \text{Probability of finding the system with position coordinates between } r^N \text{and } r^N + dr^N \text{ and spin coordinates equal to } s^N.$$

Here, $dr^N = dr_1, dr_2, ...dr_N$; $r^N = r_1, r_2.....r_N$ and s^N stands for the set $s_1, s_2.....s_N$. The spatial coordinates are continious while the spin coordinates are discrate. Because electrons are fermions and Ψ must be antisymmetric with respect to interchange of the coordinates of any two electrons. The properties of a valid wave function are: In order to avoid infinity probabilities, Ψ must be finite everywhere. In order to avoid multiple values of the probability Ψ must be single valued. For finite potentials, Ψ and $\frac{\partial \Psi}{\partial x}$ must be continious. This is required because the second order derivative term in the wave equation must be single valued. (There are exceptions to this rule when V is infinity). In order to normalize the wave functions, Ψ must approach zero as x approaches $\pm\infty$. The motion of Quantum particle can be explained with Ψ when operated with Schrödinger Equation. The product of Ψ^* and Ψ represent the probability density function [53,54]. Where Ψ^* is called the complex conjugate of Ψ. The probability of finding a particle in whole space is unity. That is,

$$\int \Psi \Psi^* dv = 1 \tag{2.2}$$

This is called normalization condition. Wave function must be continious over the full spatial range and square-integratable. There are many acceptable independent solutions of equation 2.1 for a given system. The eigenfunctions Ψ_k with corresponding energy eigenvalues are E_k. The set Ψ_k is complete and Ψ_k may always be taken to be orthonormal and normalized

$$\int \Psi_k^* \Psi_l \;\; dx^N = \;\; \langle \Psi_k | \Psi_l \rangle \;\; = \;\; \delta_{kl} \tag{2.3}$$

We denote the ground state wave function and energy by Ψ_0 and E_0. Here $\int dx^N$ means integration over $3N$ spatial coordinates and summation over N spin coordi-

nates. Expectation values of observables are given by formulas of the type,

$$\left\langle \hat{A} \right\rangle = \frac{\int \Psi^* \hat{A} \Psi \ dx}{\int \Psi^* \Psi \ dx} \tag{2.4}$$

where $\hat{A}$ is the Hermitian linear operatorfor the observable A. If Ψ is normalized, expectation values of kinetic and potential energy are given by the formulas

$$T[\Psi] = \left\langle \hat{T} \right\rangle = \int \Psi^* \hat{T} \Psi \ dx \tag{2.5}$$

$$V[\Psi] = \left\langle \hat{V} \right\rangle = \int \Psi^* \hat{V} \Psi \ dx \tag{2.6}$$

When a system is in the state Ψ, which may or may not satisfy equation 2.1, the average of many measurements of the energy is given by the formula [55]

$$E[\Psi] = \frac{\left\langle \Psi | \hat{H} | \Psi \right\rangle}{\langle \Psi | \Psi \rangle} \tag{2.7}$$

where,

$$\left\langle \Psi | \hat{H} | \Psi \right\rangle = \int \Psi^* \hat{H} \Psi dx \tag{2.8}$$

Since furthermore, each particular measurement of the energy gives one of the eigenvalues of $\hat{H}$, we immediately have

$$E[\Psi] \geq E_0 \tag{2.9}$$

The energy computed from a guessed Ψ is an upper bound to the true ground state energy E_0. Full minimization of the functional $E[\Psi]$ with respect to all allowed N-electron wave functions will give the true ground state Ψ_0 and energy $E[\Psi_0] = E_0$, that is,

$$E_0 = \min_{\Psi} \ E[\Psi]$$

Formal proof of minimum energy principle goes on follows. Expanding Ψ in terms of normalized eigenstates of $\hat{H}$

$$\Psi = \sum_k C_k \ \psi_k \tag{2.10}$$

Then the energy becomes

$$E[\Psi] = \frac{\sum_k |C_k|^2 E_k}{\sum_k |C_k|^2} \tag{2.11}$$

where E_k is the energy of the k^{th} eigenstate of $\hat{H}$. Noting that the orthogonality of the Φ_k has been used. Because $E_0 \leq E_1 \leq ...\leq E_N$. $E(\Phi)$ is always greater than or equal to E_0 and it reaches its minimum if and only if $\Psi = C_0\Psi_0$. Every eigenstate Ψ is an extremum of the function $E[\Psi]$. In other words one may replace the Schrödinger equation with the variational principle

$$\delta E[\Psi] = 0 \tag{2.12}$$

when 2.12 is satisfied, so is equation 2.1 and vice-versa.

2.1 Born-Oppenheimer approximation

In case of a many body system containing nuclius and electrons, tha Hamiltonian can be written as,

$$H = -\sum_I \frac{\hbar^2}{2m_I}\nabla^2_{R_I} - \sum_i \frac{\hbar^2}{2m_e}\nabla^2_{r_i} + \frac{1}{2}\sum_{\substack{I,J \\ I\neq J}} \frac{Z_1 Z_J e^2}{|R_I - R_J|} + \frac{1}{2}\sum_{\substack{i,j \\ i\neq j}} \frac{e^2}{|r_i - r_j|} - \sum_{I,i} \frac{Z_1 e^2}{|R_I - r_i|} \tag{2.13}$$

The first term $\sum_I \frac{\hbar^2}{2m_I}\nabla^2_{R_I}$ of the above equation represents the kinetic energy of the Nucli. Second term $\sum_i \frac{\hbar^2}{2m_e}\nabla^2_{r_i}$ represents the kinetic energy of the electrons. Third term $\frac{1}{2}\sum_{\substack{I,J \\ I\neq J}} \frac{Z_1 Z_J e^2}{|R_I - R_J|}$ is for the potential energy of nucli- nucli coulonb interaction. Fourth term $\frac{1}{2}\sum_{\substack{i,j \\ i\neq j}} \frac{e^2}{|r_i - r_j|}$is for the potential energy of electron electron coulomb interaction and the last term $\sum_{I,i} \frac{Z_1 e^2}{|R_I - r_i|}$ represents the potential energy of nucli-electron coulomb interaction.

Making use of the fact that the mass of a proton is 1838 times greater than the mass of an electron, which is the minimum mass ratio of an electron to a nucleus and becomes much higher for heavier electrons. An approximation approach that is used almost exclusively in condensed matter physics was proposed by Born and Oppenheimer in 1927. Consider the nuclei to be static, classical potentials with respect to the electrons, then address the electronic issue without further consideration of the nuclei [56]. On the timeline of the electronic transition, it is possible to claim that the core movement can be disregarded, i.e., it has no bearing on them [57–59]. Adopting Born-Oppenheimer approximation the electronic hamiltonian the becomes

$$\hat{H} = -\frac{\hbar^2}{2m}\sum_{l=1}^{N}\vec{\nabla}_l^2 + \sum_{l=1}^{N}U_{ion}(\vec{r}_l) + \sum_{l<l'}\frac{e^2}{|\vec{r}_l - \vec{r}_l'|} \tag{2.14}$$

And then the Schrödinger equation for a many body system reduces to,

$$\hat{H}\Psi = -\frac{\hbar^2}{2m}\sum_{l=1}^{N}\vec{\nabla}_l^2\psi + \sum_{l=1}^{N}U_{ion}(\vec{r}_l)\psi + \sum_{l<l'}\frac{e^2}{|\vec{r}_l - \vec{r}_l'|}\psi = E\Psi \tag{2.15}$$

Right hand site of equation 2.14 reveals that the first two terms correspond to the kinetic energies of electrons and nucli respectively. The final term in the equation represents the Hamiltonian's potential in terms of electrostatic particle-particle interactions. For issues in molecular physics and quantum chemistry, the electronic Schrödinger equation is of particular relevance. Even with all the simplicity, there are still a few critical issues that must be resolved before a workable solution can be found. The kinetic energy term in equation 2.15 is just dependent on the electron number and does not depend on the nuclear coordinate. Also the electron electron repulsion $\hat{U}$ is the same for every system with only Coulomb interaction. Therefore this also means that $\hat{T}$ and $\hat{U}$ only need the electron number as input and will therefore be denoted as universal whereas $\hat{V}$ is system dependent. The expectation value of $\hat{V}$ is also often denoted as the external potential $\hat{V}_{ext}$ which is consistent as long as there is no external electric or magnetic field present [60].

2.2 Hartree-Fock approach

The Hartree-Fock (HF) approach is the first standard approach to many body system which was applied in 1930 by Fock to atoms. The problems which are not possible to solve analitycally of many body problems, this theory gives a suitable strategy to approximate it. It is as similar as the Least Action Principle (Classical Mechanics). For now we have the interest only on the electronic Schrödinger equation. Therefore we get, $\hat{H} \equiv H_{el}, \hat{E} \equiv E_{el}$. The energy (observable) correspond to the general Hamiltonian operator can be calculated as [61],

$$E = \left\langle \hat{H} \right\rangle = \int d\vec{r}_1 \int d\vec{r}_2 ... \int d\vec{r}_N \Psi^*(\vec{r}_1, \vec{r}_2, ...\vec{r}_N) \hat{H} \Psi(\vec{r}_1, \vec{r}_2, ...\vec{r}_N) \tag{2.16}$$

If we take a wave function as a trial, the energy obtained is not the same as the actual ground state wave function. Actual ground state energy is always lower than the obtained energy. If trial wave function is equal as the ground state wave function, the energies in both cases are equal.

$$E_{trial} \geq E_o \tag{2.17}$$

with

$$E_{trial} = \int d\vec{r}_1 \int d\vec{r}_2 ... \int d\vec{r}_N \Psi^*_{trial}(\vec{r}_1, \vec{r}_2, ...\vec{r}_N) \hat{H} \Psi_{trial}(\vec{r}_1, \vec{r}_2, ...\vec{r}_N) \tag{2.18}$$

and

$$E_o = \int d\vec{r}_1 \int d\vec{r}_2 ... \int d\vec{r}_N \Psi^*_o(\vec{r}_1, \vec{r}_2, ...\vec{r}_N) \hat{H} \Psi_o(\vec{r}_1, \vec{r}_2, ...\vec{r}_N) \tag{2.19}$$

The expression above are usually inconvenient to handle. For the sake of compact notation, Dirac's Bra-ket notation [62] can be applied to the above equation as,

$$\langle \Psi_{trial} | \hat{H} | \Psi_{trial} \rangle = E_{trial} \geq E_o = \langle \Psi_o | \hat{H} | \Psi_o \rangle \tag{2.20}$$

Proof: Any normalized trial wave function Ψ_{trial} can be written as a linear combination of the Hamiltonian's eigenfunctions Ψ (each of which corresponds to an

energy eigenvalue E_i) from a complete basis set [63].

$$\Psi_{trial} = \sum_i \lambda_i \psi_i \tag{2.21}$$

The eigenfunctions are assumed to be orthogonal and normalized. Therefore, it follows that

$$\begin{aligned} \langle \Psi_{trial} | \Psi_{trial} \rangle &= 1 && (2.22)\\ &= \langle \sum_i \lambda_i \psi_i | \sum_j \lambda_j \psi_j \rangle && (2.23)\\ &= \sum_i \sum_j \lambda_i^* \lambda_j \langle \psi_i | \psi_j \rangle && (2.24)\\ &= \sum_j |\lambda_j|^2 && (2.25) \end{aligned}$$

From equation 2.21 and 2.25

$$E_{trial} = \langle \Psi_{trial} | \hat{H} | \Psi_{trial} \rangle = \langle \sum_i \lambda_i \psi_i | \hat{H} | \sum_j \lambda_j \psi_j \rangle = \sum_j E_j |\lambda_j|^2 \tag{2.26}$$

In addition to the fact that the ground state energy E_0 is by definition the lowest energy conceivable and has the lowest eigenvalue ($E_0 \leq E_i$), it is discovered that

$$E_{trial} = \sum_j E_j |\lambda_j|^2 \geq E_0 \sum_j |\lambda_j|^2 \tag{2.27}$$

One of the key ideas of density functional theory is the mathematical framework mentioned above, which consists of rules that assign numerical values to functions. In contrast to functional, which takes a function as an input and produces numerical outputs, whereas a function receives a numerical input and produces a numerical output [64]. Expressed in terms of numerical calculs where $\Psi \rightarrow N$ adresses all allowed N electron wave functions [65]

$$E_0 = \min_{\Psi \rightarrow N} \; E[\Psi] = \min_{\Psi \rightarrow N} \; \langle \Psi | \hat{H} | \Psi \rangle = \min_{\Psi \rightarrow N} \; \langle \Psi | \hat{T} + \hat{U} + \hat{V} | \Psi \rangle \tag{2.28}$$

Due to the abundance of potential wave functions and, on the other hand, the con-

strained processing capacity and time, the solution for the N electron system is almost unachievable. As in the restricted Hartree-Fock approximation, it is possible to limit the search to a more manageable subset of wavefunctions. The search is limited to the antisymetric product of N one electron wave functions that approximates N electron wavefunctions. A wave function of this type is called Slater determinant [65].

$$\Psi_0 \approx \phi_{SD} = (N!)^{-\frac{1}{2}} \begin{bmatrix} \chi_1(\vec{x}_1) & \chi_2(\vec{x}_1) & \chi_N(\vec{x}_1) \\ \chi_1(\vec{x}_2) & \chi_2(\vec{x}_2) & \chi_N(\vec{x}_2) \\ \vdots & \vdots & \vdots \\ \chi_1(\vec{x}_N) & \chi_2(\vec{x}_N) & \chi_N(\vec{x}_N) \end{bmatrix} \tag{2.29}$$

It is crucial to note that the spin orbitals $\chi_i(\vec{x}_i)$ depend on spin coordinates as well as spatial coordinates. Spin coordinates are introduced by the spin function $\vec{x}_i = \vec{r}_i, s$. The text by Szabo [66] and Holthausen [67] omits a thorough description of the spin orbitals and their characteristics. Going back to the variational principle and equation 2.26, the ground state energy that can be roughly predicted by a single determinant becomes

$$E_0 = \min_{\phi_{SD} \to N} E[\phi_{SD}] = \min_{\phi_{SD} \to N} \langle \phi_{SD} | \hat{H} | \phi_{SD} \rangle = \min_{\phi_{SD} \to N} \langle \phi_{SD} | \hat{T} + \hat{U} + \hat{V} | \phi_{SD} \rangle \tag{2.30}$$

A general expression for the Hartree-Fock energy is obtained by uses of the slatter determinant as a trial function. According to equation 2.22, the normalization integral $\langle \Psi_{HF} | \Psi_{HF} \rangle$ is equal to 1 and the energy expectation value is found to be given by the formula

$$E_{HF} = \langle \Psi_{HF} | \hat{H} | \Psi_{HF} \rangle = \sum_{i=1}^{N} H_i + \frac{1}{2} \sum_{i,j=1}^{N} (J_{ij} - K_{ij}) \tag{2.31}$$

where

$$H_i = \int \psi_i^*(x) [-\frac{1}{2} \vec{\nabla}^2 + U(x)] \psi_i(x) \quad dx \tag{2.32}$$

$$J_{ij} = \int \int \psi_i(x_1) \psi_i^*(x_1) \frac{1}{r_{12}} \psi_j^*(x_2) \psi_j(x_2) \quad dx_1 dx_2 \tag{2.33}$$

$$K_{ij} = \int\int \psi_i(x_1)\psi_j(x_1)\frac{1}{r_{12}}\psi_i(x_2)\psi_j^*(x_2) \quad dx_1 dx_2 \tag{2.34}$$

These integrals are all real and $J_{ij} \geq K_{ij} \geq 0$. J_{ij} are called Coulomb integrals and K_{ij} are exchange integrals. We have the important equation

$$J_{ii} = K_{ii} \tag{2.35}$$

This is the reason the double summation in the equation that include $i = j$ terms. Minimization of equation subject to the orthonormalization conditions,

$$\int \psi_i^*(x)\psi_j(x) \quad dx = \delta_{ij}$$

gives the Hartree-Fock differential equation

$$\hat{F}\Psi_i(x) = \sum_{j=1}^{N} \varepsilon_{ij}\psi_j(x) \tag{2.36}$$

Where

$$\hat{F} = -\frac{1}{2}\vec{\nabla}^2 + \vec{v} + \vec{g} \tag{2.37}$$

In which the Coulomb exchange operator $g(x_1)$ is given by

$$\vec{g} = \hat{j} - \hat{k} \tag{2.38}$$

Here

$$J(x_1)f(x_1) = \sum_{k=1}^{N} \int \psi_k^*(x_2)\psi_k(x_2)\frac{1}{r_{12}}f(x_1) \quad dx_2 \tag{2.39}$$

$$K(x_1)f(x_1) = \sum_{k=1}^{N} \int \psi_k^*(x_2)f(x_2)\frac{1}{r_{12}}\psi_k(x_1) \quad dx_2 \tag{2.40}$$

with $f(x_1)$ an arbitrary function. The matrix ε consists of lagrange multipliers. Also,

$$\varepsilon_{ji}^* = \varepsilon_{ij} \tag{2.41}$$

where ε is Hermitian. Now multiplying equation 2.31 with Ψ_i^* and integrating, one

obtains the formula for orbital energies

$$\varepsilon_i \equiv \varepsilon_{ii} = \langle \psi_i | \hat{F} | \psi_i \rangle = H_i + \sum_{j=1}^{N} (\vec{J}_{ij} - \vec{K}_{ij}) \tag{2.42}$$

Summing over i and compearing with equation 2.34 we get,

$$E_{HF} = \sum_{i=1}^{N} \varepsilon_i - \hat{V}_{ee} \tag{2.43}$$

Where the symbol V_{ee} stands for electron electron repulsion energy.

$$\hat{V}_{ee} = \int \psi^*_{HF}(x^N) \left(\sum_{i<j} \frac{1}{r_{ij}} \right) \psi_H \left(x^N \right) \quad dx^N \tag{2.44}$$

$$= \frac{1}{2} \sum_{i,j=1}^{N} (\vec{J}_{ij} - \vec{K}_{ij}) \tag{2.45}$$

For the total molecular energy including nucleus nucleus repulsion one has,

$$W_{HF} = \sum_{i=j}^{N} \varepsilon_i - \hat{V}_{ee} + \hat{V}_{nn} \tag{2.46}$$

$$= \sum_{i=j}^{N} H_i + \hat{V}_{ee} + \hat{V}_{nn} \tag{2.47}$$

Nither E_{HF} nor W_{HF} is equal to the sum of orbital energies. Hartree-Fock method is a non-linear self-consistent field.

2.3 Limitations of HF approach

When the even number of electrons are located in double occupied spatial orbital, it is called that the compound is in singlet state. It also called closed-shell system. Again having odd number of electrons (compound with single occupied orbital) is called triplet state. It also called open shell system. This two types of system gives us two different approaches of Hartree-Fock methood. In restricted HF (RHF) methood, all electrons are considered to be paired where as in UHF method, this restriction is lifted totally. All electrons are regarded as being coupled in orbitals

in the restricted HF method (RHF), but this restriction is completely eliminated in the unrestricted HF method (UHF). Open-shell systems can also be described using the restricted open-shell HF (ROHF) method, which is more difficult and thus less common than UHF. In this method, only the single occupied orbitals are eliminated.

Additionally, there are closed-shell systems that need an open strategy to produce the desired outcomes. For example, using a system that places both electrons in the same spatial orbital would logically make it impossible to describe the dissociation of H_2 (i.e., the behavior at large internuclear distance), where one electron must be situated at each hydrogen atom. This means that in HF calculations, the method selection is always a crucial factor [68]. The size of the investigated system is a limiting factor for calculation. Kohn states $M = p^5$ with $3 \leq p \leq 10$ parameters for the result with sufficient accuracy in investigation of H_2 system. When $N = 100$ electrons are present, the number of parameters increases to,

$$M = p^{3N} = 3^{300} \rightarrow 10^{300} \approx 10^{150} \rightarrow 10^{300} \tag{2.48}$$

Equation 2.48 states that the energy minimization would need to be carried out in a space with at least 10^{150} dimensions, which is considerably above current processing capabilities. Therefore, HF-methods are limited to systems with few involved electrons ($N \approx 10$). This restriction is commonly referred to as the exponential wall because of the exponential factor in equation 2.45 [69]. The energy determined by HF calculations is never exactly the same as the ground state energy because a many electron wave function cannot be completely represented by a single Slater determinant. The Hartree-Fock-limit is the most precise energy that can be calculated using HF-methods [67].

2.4 Correlation energy

No single determinant or straightforward combination of a few determinants can ever accurately describe the wave function for a system with many interacting electrons. The calculation of the energy error, however, is here characterized as being

negative. The difference between E_{HF} and E_{exact} is called correlation energy and can be denoted as [70],

$$E_{corr}^{HF} = E_{min} - E_{HF} \tag{2.49}$$

When atomic and molecular changes preserve the number and type of chemical bonds, correlation energy tends to remain constant, but it can fluctuate significantly and become decisive when bonds change. Its magnitude can range from a few hundredths of an atomic unit to hundreds of kilocalories per mole. Exchange energies are an order magnitude or more bigger, even if the self exchange term is omitted. Despite the fact that E_{corr} is usually small against E_{min} as in the example of a N_2 molecule where

$$E_{corr}^{HF} = 14.9\ eV \quad \langle \quad 0.001 \quad E_{min} \tag{2.50}$$

It can have a huge influence. For instance, the experimental dissociation energy of the N_2 molecule is,

$$E_{diss} = 9.9\ eV \quad \langle \quad E_{corr} \tag{2.51}$$

which corresponds to a large contribution of the correlation energy to relative energies which are of particular interest in quantum chemistry [71]. The mean field approximation utilized in the HF-method is what contributes most to the correlation energy. The implication of this is that one electron moves in the average field of the other ones, a method that completely ignores the inherent correlation of the electron movements. To get a better understanding what that means, one may picture the repulsion of electrons at small distances which clearly cannot be covered by a mean-field approach like the Hartree-Fock-method.

Chapter 3

Density Functional Theory

In an electronic system, the number of electrons per unit volume in a given state is the electron density for a state designated by $\rho(r)$. Its formula in terms of Ψ is

$$\rho(r_1) = N \int ... \int |\psi(x_1, x_2....x_N)|^2 \quad ds_1 dx_2 ... dx_N \tag{3.1}$$

This is a non negative simple function of three variables x, y, z integrating to the total number of electrons,

$$N = \int \rho(r) \quad dr \tag{3.2}$$

For an atom in its ground state the density decreases monotonically away from the nucleus [72]. The electron density at any atomic nucleus in an atom, molecule, or solid has a finite value. Hohenberg and Kohn pointed out that if one knows the density of the ground state of a many electron system, one can deduce from it the external potential in which the electrons reside, up to an overall constant [73]. It must be kept in mind that the only ways in which two many electron problem can differ are in the external potentials U and in the number of electrons that reside in the potentials. According to this results, both of these external parameters are determined by the electron density, so one can say that the density completely determines the many body problem. This statement is surprising, because the density is

a real function of a single spatial variable while complete quantum mechanical wave function needs N variables for its description. The starting point of the theory is the observation of Hohenberg and Kohn that electron density contains in principle all the information contained in a many electron wave function. The electronic density of a many electron system at point $\vec{r}$ is defined to be

$$n(\vec{r}) = \langle\Psi| \sum_{l=1}^{N} \delta(\vec{r} - \vec{R}_l)|\Psi\rangle \tag{3.3}$$

$$= N \int d\vec{r}_1....d\vec{r}_N \;\; \Psi^*(\vec{r}_1, \vec{r}_2....\vec{r}_N) \;\; \delta(\vec{r} - \vec{r}_l) \;\; \Psi(\vec{r}_1....d\vec{r}_N) \tag{3.4}$$

3.1 Thomas-Fermi model

The assumptions stated by Thomas are that, electrons are distributed uniformly in a six dimentional phase space for the motion of an electron at the rate of two for each h^3 of volume and that there is an effective potential field that is itself determined by the nuclear charge and this distribution of electrons. The Thomas Fermi formula for electron density can be derived from these assumptions [73]. Let us consider the space devided into many small cubes, each of side l and volume $\Delta V = l^3$, each containing some fixed number of electrons ΔN and we assume that the electrons in each shell behave like indipendent fermions at the temperature 0K, with the cells independent of one another. The energy level of a particle in a three dimensional infinite well are given by the formula [73]

$$\varepsilon\left(n_x, n_y, n_z\right) = \frac{h^2}{8ml^2}\left(n_x^2 + n_y^2 + n_z^2\right) \tag{3.5}$$

$$= \frac{h^2}{8ml^2} R^2 \tag{3.6}$$

Where $n_x, n_y, n_z = 1, 2, 3...$ and the second equality defines by the quantity R. For high quantum numbers, that is, for large R, the number of distinct energy levels with energy smaller than ε can be approximated by the volume of one octant of a

spherical with radius R in the space (n_x, n_y, n_z). This number is,

$$\phi(\varepsilon) = \frac{1}{8}\left(\frac{4\pi R^3}{3}\right) \qquad \left[\because R = \left(\frac{8ml^2\varepsilon}{h^2}\right)^{\frac{3}{2}}\right] \tag{3.7}$$

$$= \frac{\pi}{6}\left(\frac{8ml^2\varepsilon}{h^2}\right)^{\frac{3}{2}} \tag{3.8}$$

The number of energy levels between ε and $\varepsilon + \delta\varepsilon$ is accordingly

$$g(\varepsilon)\Delta\varepsilon = \phi(\varepsilon + \delta\varepsilon) - \phi(\varepsilon) \tag{3.9}$$

$$= \frac{\pi}{4}\left(\frac{8ml^2\varepsilon}{h^2}\right)^{\frac{3}{2}\varepsilon^{\frac{1}{2}}} \delta\varepsilon + O\left((\delta\varepsilon)^2\right) \tag{3.10}$$

where the function $g(\varepsilon)$ is the density of states at energy ε. To compute the total energy for the cell with ΔN electrons, we need the probability for the state with energy ε to be occupied which we call $f(\varepsilon)$. This is the Fermi Dirac distribution.

$$f(\varepsilon) = \frac{1}{1 + e^{\beta(\varepsilon - \mu)}} \tag{3.11}$$

which at 0K reduces to a step function:

$$f(\varepsilon) = \begin{cases} 1 & \varepsilon \ \langle \ \varepsilon_f \\ 0 & \varepsilon \ \langle \ \varepsilon_f \end{cases} \qquad as \quad \beta \to 0$$

where ε_f is the Fermi energy. All the states energy smaller than ε_f are occupied and those with energy greater than ε_f are occupied. The Fermi energy ε_f is the zero temperature limit of the chemical potential μ. Now we find the total energy of the electrons in this cell by summing the contributions from the different energy states:

$$\Delta E = 2\int \varepsilon\, f(\varepsilon)\, g(\varepsilon)\, d\varepsilon \tag{3.12}$$

$$= 2\int \varepsilon\, f(\varepsilon)\, \frac{\pi}{4}\left(\frac{8ml^2}{h^2}\right)^{\frac{3}{2}\varepsilon^{\frac{1}{2}}} d\varepsilon \tag{3.13}$$

$$= \frac{8\pi}{5}\left(\frac{2m}{h^2}\right)^{\frac{3}{2}} l^3 \varepsilon_f^{\frac{5}{2}} \tag{3.14}$$

where the factor 2 enters because each energy level is doubly occupied by one electron with spin α and another with spin β. The fermi energy E_f is related to the number of electrons ΔN in the cell through the formula

$$\Delta N = 2 \int f(\varepsilon)\, g(\varepsilon)\, d\varepsilon \tag{3.15}$$

$$= \frac{8\pi}{3} \left(\frac{2m}{h^2}\right)^{\frac{3}{2}} l^3 \varepsilon_f^{\frac{3}{2}} \tag{3.16}$$

Eleminating ε_f from 3.15 and 3.16 we have

$$\Delta E = \frac{3}{5}\, \Delta N\, E_f \tag{3.17}$$

$$= \frac{3h^2}{10m} \left(\frac{3}{8\pi}\right)^{\frac{2}{3}} l^3 \left(\frac{\Delta N}{l^3}\right)^{\frac{5}{3}} \tag{3.18}$$

Equation 3.18 is a relation between total kinetic energy and the electron density $\rho = \frac{\Delta N}{l^3} = \frac{\Delta N}{\Delta V}$ for each cell in the space. Adding the contribution from all cells we find the total kinetic energy to be, now reverting to atomic units,

$$T_{TF}[\rho] = C_F \int \rho^{\frac{5}{3}}(\vec{r})\, d\vec{r} \tag{3.19}$$

where

$$C_F = \frac{3}{10} \left(3\pi^2\right)^{\frac{2}{3}} = 2.871 \tag{3.20}$$

Here, we first come across the LDA [74], one of the most significant concepts in contemporary density functional theory. By using locally applicable relations suited for a homogeneous electronic system, electronic characteristics are approximated as functions of the electron density. In terms of electron density, the energy formula for an atom is

$$T_{TF}[\rho(\vec{r})] = C_F \int \rho^{\frac{5}{3}}(\vec{r})\, d\vec{r} - Z \int \frac{\rho(\vec{r})}{\vec{r}} d\vec{r} + \frac{1}{2} \iint \frac{\rho(\vec{r}_1)\rho(\vec{r}_2)}{|\vec{r}_1 - \vec{r}_2|}\, d\vec{r}_1 d\vec{r}_2 \tag{3.21}$$

This is the energy functional of Thomas-Fermi theory of atoms. The method became considered as an overly simplified model of little real significance for quantitative predictions in atomic, molecular, or solid state physics because the accuracy for

atoms is not as high with this model as it is with other methods.

3.2 Hohenberg-Kohn Theorem

For an electronic system described by the Hamiltonian

$$\hat{H} = \sum_{i=1}^{N}(-\frac{1}{2}\vec{\nabla}_i)^2 + \sum_{i=1}^{N} V(\vec{r}_i) + \sum_{i<j}^{N} \frac{1}{\vec{r}_{ij}} \tag{3.22}$$

both the ground state energy and the ground state wave function are determined by the minimization of energy functional $E[\Psi]$.

$$E[\Psi] = \frac{\left\langle \Psi|\hat{H}|\Psi \right\rangle}{\langle \Psi|\Psi \rangle}, \qquad E[\Psi] \geq E_0 \tag{3.23}$$

But for an N electron system, the external potential $v(\vec{r})$ completely fixes the Hamiltonian, thus N and $v(\vec{r})$ determines all properties for the ground state.

3.2.1 Theorem 1

First Hohenberg-Khon theorem legitimizes the use of electron density $\rho(\vec{r})$ as basic variable. Since ρ determines the number of electrons, it follows that $\rho(\vec{r})$ also determines the ground state wave function Ψ and all other electronic properties of the system. Where $v(\vec{r})$ is not restricted to coulomb potential. It states

Statement: The external potential $v(\vec{r})$ is determined within a trival additive constant by the electron density $\rho(\vec{r})$. [72]

Proof: The proof of this theorem of Hohenberg and Khon is desarmingly simple. Al that is employed is the minimum energy principle for the ground state. Let us consider the electron density $\rho(\vec{r})$ for the non degenerated ground state of some N electron system. It determines N by simple quardrature. It also determines $v(\vec{r})$ hence all the properties of the system. For if there were two external potentials v and v' differing by more than a constant, each giving the same ρ for its ground state. We would have two Hamiltonians H and H' whose ground state densities are same

althrough the normalized wave functions Ψ and Ψ' would be different. Taking Ψ as a trial function for the H problem, we would have then from 3.24

$$E_o \quad \langle \quad \langle \Psi' | H | \Psi' \rangle = \langle \Psi' | H' | \Psi' \rangle + \langle \Psi' | H - H' | \Psi' \rangle \tag{3.24}$$

$$= E_0' + \int \rho(\vec{r}) \, [v(\vec{r}) - v'(\vec{r})] \, d\vec{r} \tag{3.25}$$

where E_o and E_o' are the ground state energies for H and H' respectively. Similarly taking Ψ as trial function for the H' problem

$$E_o' \quad \langle \quad \langle \Psi | H' | \Psi \rangle = \langle \Psi | H | \Psi \rangle + \langle \Psi | H' - H | \Psi \rangle \tag{3.26}$$

$$= E_0 - \int \rho(\vec{r}) \, [v(\vec{r}) - v'(\vec{r})] \, d\vec{r} \tag{3.27}$$

From equation 3.25 and 3.27,

$$E_0 + E_0' \quad \langle \quad E_0' + E_0 \tag{3.28}$$

Its a contradiction. So there can not be two different v that give the same ρ for there ground state. Thus ρ determines N and v and hence all properties of the ground state, for example the kinetic energy $T[\rho]$ the potential energy $V[\rho]$ and the total energy $E[\rho]$. So the writting E_v for E to make explicit the dependence on V.

$$E_v[\rho] = T[\rho] + V_{ee}[\rho] + V_{ne}[\rho] \tag{3.29}$$

$$= F_{HK}[\rho] + \int \rho(\vec{r}) v(\vec{r}) \, d\vec{r} \tag{3.30}$$

Where

$$F_{HK}[\rho] = T[\rho] + V_{ee}[\rho] \tag{3.31}$$

We may write

$$V_{ee}[\rho] = \text{J } [\rho] + \text{non-classical term}$$

Where $J[\rho]$ is the classical repulsion that can be represented as,

$$J[\rho] = \frac{1}{2} \iint \frac{1}{\vec{r}_{12}} \, \rho(\vec{r}_1) \rho(\vec{r}_2) \, d\vec{r}_1 d\vec{r}_2 \tag{3.32}$$

The nonclassical term is a very exclusive term. It is the major part of exchange correlation energy.

3.2.2 Theorem 2

The second Hohenberg Khon theorem provides the energy variational principle. It reads:

Statement: For a trial density $\rho(\vec{r})$, such that $\rho(\vec{r}) \geq 0$ and $\int \rho(\vec{r})\ \mathrm{d}\vec{r} = N$

$$E_0 \leq E_v[\rho] \tag{3.33}$$

Where $E_v[\rho]$ is the energy functional. Originally this second theorem has been proved by variation calculus, [75] the proof provided subsequently is a different one, namely the so called constrained-search approach, introduced by Levy and Lieb [6, 7] and subsequently thoroughly examined in the books by Parr, Yang as well as Kryachko and Ludena [76, 77].

Proof: The previous theory assures that $\tilde{\rho}$ determines its own $\tilde{v}$, Hamiltonian $\tilde{H}$, and wave function $\tilde{\Psi}$, which can be taken as a trial function for the problem of interest having external potential v. Thus,

$$\left\langle \tilde{\Psi}|\hat{H}|\tilde{\Psi} \right\rangle = \int \tilde{\rho}(\vec{r})v(\vec{r}) + F_{HK}[\tilde{\rho}] = E_v[\tilde{\rho}] \geq E_v[\rho] \tag{3.34}$$

Assuming differentiability of $E_v[\rho]$, the variation principle requires that the ground state density satisfy the stationary principle

$$\delta\{E_v[\rho] - \mu[\int \rho(\vec{r})d\vec{r} - N]\} = 0 \tag{3.35}$$

Which gives the Euler-Lagrange equation,

$$\mu = \frac{\delta E_v[\rho]}{\delta\rho(\vec{r})} = v(\vec{r}) + \frac{\delta F_{HK}[\rho]}{\delta\rho(\vec{r})} \tag{3.36}$$

The quantity μ is the chemical potential. If we know the exact $F_{HK}[\rho]$, above equa-

tion could be an exact equation for the ground state electron density. When we say that all ground state properties are functionals of electron density, we need to understandthese functionals are defined only for v representable densities of particular importance is the functional $F_{HK}[\rho]$ of $F_{HK}[\rho] = T[\rho] + V_{ee}[\rho]$,

$$F_{HK}[\rho] = \langle \Psi | T + V_{ee} | \Psi \rangle \tag{3.37}$$

Where, Ψ is the ground state wave function associated with ρ, which has to be v-representable. The second Hohenberg-Khon theory simply states that for all v-representale densities.

$$E_v[\rho] \equiv F_{HK}[\rho] + \int \rho(\vec{r}) v(\vec{r})\, d\vec{r} \geq E_v[\rho_0] \tag{3.38}$$

Where, $E_v[\rho_0]$ is the ground state energy of the Hamiltonian with $v(\vec{r})$ as external potential and ρ_0 is the ground state density. So the minimum energy principle for the ground state gives,

$$\left\langle \Psi_{\rho_0} | \hat{H} | \Psi_{\rho_0} \right\rangle \quad \geq \quad \left\langle \Psi_0 | \hat{H} | \Psi_0 \right\rangle \tag{3.39}$$

3.3 Kohn-Sham Equation

Kohn and Sham proposed introducing orbitals into the problem in such a way that the kinetic energy can be computed simply to good accuracy leaving a small residual correction that is handeled seperately. To understand what is involved and what khon Sham did, it is convenient to begin with the exact formula for the ground state kinetic energy.

$$T = \sum_{i}^{N} n_i \left\langle \psi_i | -\frac{1}{2} \vec{\nabla}^2 | \psi_i \right\rangle \tag{3.40}$$

Where ψ_i and n_i are respectively, natural spin orbitals and there occupation numbers. The pauli principle requires that $0 \leq n_i \leq 1$. We are assured from the Hohen-

berg Khon theory theory that T is a functional of he total energy density.

$$\rho(\vec{r}) = \sum_{i}^{N} n_i \sum_{s} |\psi_i(\vec{r}, \vec{s})|^2 \tag{3.41}$$

For any interacting system of interest, there are an infinite number of terms in equation 3.40 and 3.41 which is ponderous at best. Kohn and Sham showed that one can build a thory using simplier formulas, namely

$$T_s[\rho] = \sum_{i}^{N} \left\langle \psi_i | -\frac{1}{2}\vec{\nabla}^2 | \psi_i \right\rangle \tag{3.42}$$

and

$$\rho(\vec{r}) = \sum_{i}^{N} \sum_{s} |\psi_i(\vec{r}, \vec{s})|^2 \tag{3.43}$$

Equation 3.42 and 3.43 are the special cases of equation 3.40 and 3.41 having n_i=1 for N orbitals and n_i= 0 for the rest. This representation of Kinetic energy and density holds true for the determinental wave function that exactly describes N non interacting electrons. We know that, any normalized and continious non negative density is N representable and always can be decomposed according to equation 3.43. But given a $\rho(\vec{r})$, how can we have a unique decomposition in terms of orbitals so as to give a unique value to $T_s[\rho]$ through equation 3.42. In analogy with the Hohenberg-Khon definition of the universal functional $F_{HK}[\rho]$ Khon and Sham invoked a corresponding non interacting reference system with the Hamiltonian

$$\hat{H}_s = \sum_{i}^{N} \left(-\frac{1}{2}\vec{\nabla}_i^2 \right) + \sum_{i}^{N} v_s(\vec{r}) \tag{3.44}$$

In which there are no electron electron repulsion terms and for which the ground state electron density is exactly ρ. For this system there will be an exact determinantal ground state wave function

$$\Psi_s = \frac{1}{\sqrt{N!}} \quad det\ [\psi_1, \psi_2 ..... \psi_N] \tag{3.45}$$

And the ψ_i are the N lowest eigenstates of the electron electron Hamiltonian H_s:

$$\hat{H}_s\psi_i = [-\frac{1}{2}\nabla^2 + V_s(\vec{r})]\psi_i = \varepsilon_i\psi_i \tag{3.46}$$

The Kinetic energy is $T_s[\rho]$, given by equation 3.42

$$T_s[\rho] = \left\langle \psi_s | \sum_i^N (-\frac{1}{2}\vec{\nabla}_i^2) | \psi_s \right\rangle \tag{3.47}$$

$$= \sum_i^N \left\langle \psi_i | -\frac{1}{2}\vec{\nabla}_i^2 | \psi_i \right\rangle \tag{3.48}$$

and the density is decomposed as in equation 3.43. The forgoing definition of $T_s[\rho]$ leaves an undesirable restriction on the density. Its need to be non interacting v representable. That is, there must exist a non interacting ground ground state with the given density $\rho(\vec{r})$. This restriction on the domain of definition of $T_s[\rho]$ can be lifted and $T_s[\rho]$ of the form of equation 3.42 can be defined for any density derived from an anti-symmetric wave function. The quantity $T_s[\rho]$, althrough uniquely defined for any density, its not still the kinetic energy functional $T[\rho]$. The very clear idea of Khon and Sham is to set up a problem of interest in such a way that $T_s[\rho]$ is its kinetic energy component exactly. The resultant theory turns out to be of independent particle form.

$$E_{xc}[\rho] = T[\rho] - T_s[\rho] + V_{ee}[\rho] - J[\rho] \tag{3.49}$$

The defined quantity $E_{xc}[\rho]$ is called the exchange correlation energy. It contains the difference between T and T_s, presumably fairly small and the non classical part of $V_{ee}[\rho]$. The Euler equation then can be written in terms of effective potential.

$$\mu = v_{eff}(\vec{r}) + \frac{\delta T_s[\rho]}{\delta\rho(\vec{r})} \tag{3.50}$$

Where Khon Sham effective potential is defined by,

$$v_{eff}(\vec{r}) = v(\vec{r}) + \frac{\delta J[\rho]}{\delta\rho(\vec{r})} + \frac{\delta E_{xc}[\rho]}{\delta\rho(\vec{r})} \tag{3.51}$$

$$= v(\vec{r}) + \int \frac{\rho(\vec{r'})}{|\vec{r} - \vec{r'}|} + V_{xc}(\vec{r}) \tag{3.52}$$

Where $V_{xc}(\vec{r}) = \frac{\delta E_{xc}[\rho]}{\delta\rho(\vec{r})}$ is the exchange correlation potential. Equation 3.52 with the constraints $\int \rho(\vec{r})d(\vec{r}) = N$ is precisely the same equation as one obtains from conventional density functional theory when one applies it to a system of non interacting electrons moving in an external potential $V_s(\vec{r}) = V_{eff}(\vec{r})$. For a given $v_{eff}(\vec{r})$, one obtains the $\rho(\vec{r})$ that satisfies equation 3.52 simply by solving the N one electron equations.

$$[-\frac{1}{2}\vec{\nabla}^2 + V_{eff}(\vec{r})]\ \psi_i = \varepsilon_i\psi_i \tag{3.53}$$

and setting

$$\rho_(\vec{r}) = \sum_i^N \sum_s |\psi_i(\vec{r}, \vec{s})|^2 \tag{3.54}$$

In above two equations the solutions ψ_i can be different this is because equations are non linear and must be solved iteratively. The total energy can be determined from the resultant density via equation

$$E[\rho] = T_s[\rho] + J[\rho] + E_{xc}[\rho] + \int \rho(\vec{r})V(\vec{r})d\vec{r} \tag{3.55}$$

$$E[\rho] = \sum_i^N \sum_s \int \psi_i^*(\vec{r})(-\frac{1}{2}\vec{\nabla}_i^{\,2})\psi_i(\vec{r})d\vec{r} + J[\rho] + E_{xc}[\rho] + \int \rho(\vec{r})V(\vec{r})d\vec{r} \tag{3.56}$$

Hence,

$$\sum_i^N \varepsilon_i = \sum_i^N + \left\langle \psi_i| -\frac{1}{2}\vec{\nabla}^2 + V_{eff}(\vec{r})|\psi_i \right\rangle \tag{3.57}$$

$$= T_s[\rho] + \int V_{eff}(\vec{r})\rho(\vec{r})d\vec{r} \tag{3.58}$$

Just as in Hartree-Fock theory, the total electronic energy is not the sum of the orbital energies.

3.3.1 Solving Khon-Sham equation

In a condensed matter system the KS equation gives a way to obtain the exact density and energy of the ground state. The process starts with an initial electron density $n(r)$, usually a superposition of atomic electron density, then the effective KS potential V_{KS} is calculated and the KS equation is solved with single-particle eigenvalues and wavefunctions, a new electron density is then calculated from the wavefunctions.

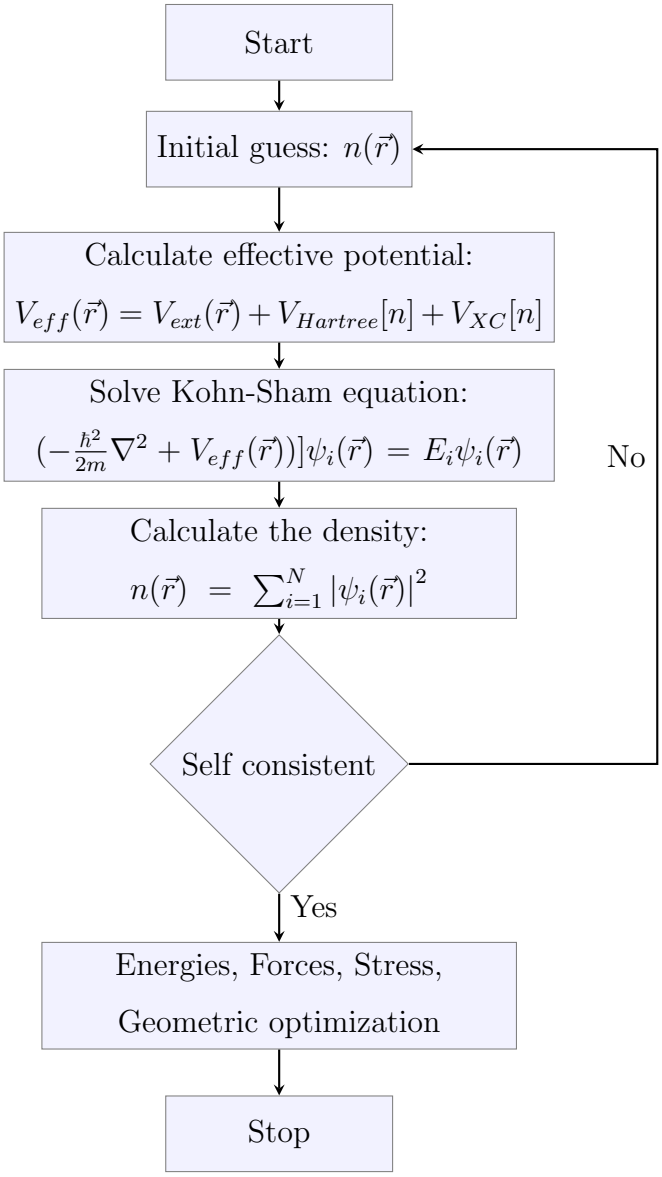

This is usually done numerically through some self consistent iteration as shown in above flowchart. Self-consistent condition(s) can be the change of total energy or

electron density from the previous iteration or total force acting on atoms is less than some chosen small quantity, or a combination of these individual conditions. If the self-consistency is not achieved, the calculated electron density will be mixed with electron density from previous iterations to get a new electron density. A new iteration will start with the new electron density. This process continues until self-consistency is reached. After the self-consistency is reached, various quantities can be calculated including total energy, forces, stress, eigenvalues, electron density of states, band structure, etc..

3.4 Local Density Approximation (LDA)

The Khon Sham equation while exactly incorporating the kinetic energy $T_s[\rho]$, still leave the exchange correlational functional $E_{xc}[\rho]$ unsetteled. In Khon Sham equation let us introduce the local density approximation proposed by Khon and Sham. The kinetic energy $T_s[\rho]$ is regorously treated in the Kohn Sham schame, we can use the uniform electron gas formula solely for the unknown part of the rest of the energy functional. Thus we introduce the local density approximation (LDA) for exchange and correlation energy.

$$E_{xc}^{LDA}[\rho] = \int \rho(\vec{r})\varepsilon_{xc}(\rho)\, d\vec{r} \tag{3.59}$$

Where $\varepsilon_{xc}[\rho]$ indicates the exchange and correlation energy per particle of a uniform electron gas of density ρ. The corresponding exchange correlation potential then becomes,

$$V_{xc}^{LDA}(\vec{r}) = \frac{\delta E_{xc}^{LDA}[\rho]}{\delta\rho(\vec{r})} \tag{3.60}$$

$$= \varepsilon_{xc}(\rho(\vec{r})) + \rho(\vec{r})\, \frac{\delta E_{xc}[\rho]}{\delta\rho(\vec{r})} \tag{3.61}$$

and the Khon Sham orbital equations read,

$$[-\frac{1}{2}\vec{\nabla}^2 + V(\vec{r}) + \int \frac{\rho(\vec{r'})}{|\vec{r} - \vec{r'}|} d\vec{r'} + V_{xc}^{LDA}(\vec{r})]\Psi = \varepsilon_i \Psi_i \tag{3.62}$$

This self consistent solution defines the KS local density approximation, which is the literature is usually simply called Local Density Approximation (LDA) method. The function $\varepsilon_{xc}(\rho)$ can be devided into exchange and correation contributions,

$$\varepsilon_{xc}(\rho) = \varepsilon_x(\rho) + \varepsilon_c(\rho) \tag{3.63}$$

The exchange part is already known given by the Dirac exchange energy functional.

$$\varepsilon_x(\rho) = -C_x \ \rho^{\frac{1}{3}}(\vec{r}) \tag{3.64}$$

where

$$C_x = \frac{3}{4}\left(\frac{3}{\pi}\right)^{\frac{1}{3}} \tag{3.65}$$

3.5 Local Spin Density Approximation (LSDA)

The spin density functional theory is the necessary generalization for the system in the presence of an external magnetic field. It is also exceedingly important for the systems in the absence of a magnetic field, because it allows one to build more physics into the exchange correlation functional through its spin dependence. In the presence of a magnetic field $B(\vec{r})$ that acts only on the spins of the electrons, the Hamiltonian of the system then becomes

$$H = -\frac{1}{2}\sum_{i}^{N}\vec{\nabla}_i^2 + \sum_{i}^{N} V(\vec{r_i}) + \sum_{i<j}^{N}\frac{1}{\vec{r_{ij}}} + 2B_e\sum_{i}^{N} B(\vec{r}).S_i \tag{3.66}$$

Where, $B_e = \frac{e\hbar}{2mc}$ is the Bohr magneton and S_i is the electron angular momentum vector for the i^{th} electron. The added magnetic interaction is still a one-electron operator, just like the nuclear potential $V(\vec{r})$. We can combine turms in the following convenient way,

$$\hat{V} = \sum_{i}^{N} V(\vec{r_i}) + 2B_e\sum_{i}^{N} B(\vec{r}).S_i \tag{3.67}$$

$$= \int v(\vec{r})\rho(\vec{r})d\vec{r} - \int B(\vec{r})m(\vec{r})d\vec{r} \tag{3.68}$$

Where $\rho(\vec{r})$ is the operator for electron density

$$\rho(\vec{r}) = \sum_{i}^{N} \delta(\vec{r} - \vec{r_i}) \tag{3.69}$$

and $m(\vec{r})$ is the operator for the electron magnetization density.

$$m(\vec{r}) = -2B_e \sum_{i}^{N} S_i \ \delta(\vec{r} - \vec{r_i}) \tag{3.70}$$

Both $\rho(\vec{r})$ and $m(\vec{r})$ are local operators. The expectation value of V for the state $|\Psi\rangle$ is given by

$$\left\langle \Psi|\hat{V}|\Psi \right\rangle = \int v(\vec{r})\rho(\vec{r})d\vec{r} - \int B(\vec{r})m(\vec{r})d\vec{r} \tag{3.71}$$

when the electron density is given by

$$\rho(\vec{r}) = \langle \Psi|\rho(\vec{r})|\Psi\rangle \tag{3.72}$$

and the magnetization density by,

$$m(\vec{r}) = \langle \Psi|m(\vec{r})|\Psi\rangle \tag{3.73}$$

We shall discuss only the simple case of z direction $b(\vec{r})$. We then have

$$\left\langle \Psi|\hat{V}|\Psi \right\rangle = \int v(\vec{r})\rho(\vec{r})d\vec{r} - \int b(\vec{r})m(\vec{r})d\vec{r} \tag{3.74}$$

where

$$m(\vec{r}) = -2B_e \left\langle \Psi| \sum_{i}^{N} S_z(i)\delta(\vec{r} - \vec{r_i})|\Psi \right\rangle \tag{3.75}$$

$$= -2B_e \int S_z(i)\delta(\vec{r} - \vec{r_i})\ \gamma_1(x', x')\ dx' \tag{3.76}$$

$$= -2B_e \sum_{s=\alpha,\beta} S_z\ \gamma_1(\vec{r_s}, \vec{r_s}) \tag{3.77}$$

$$= -2B_e\ [\frac{1}{2}\gamma_1(\vec{r}_\alpha, \vec{r}_\alpha) + (-\frac{1}{2})\gamma_1(\vec{r}_\beta, \vec{r}_\beta)] \tag{3.78}$$

$$= B_e\ \rho_\beta(\vec{r}) - \rho_\alpha(\vec{r})] \tag{3.79}$$

We obtain the spin density functional theory by breaking the minimum search for the ground state energy into two steps, namely

$$\begin{aligned} E_0 &= \min_{\Psi} \left\langle \Psi | T + V_{ee} + \sum_i^N U(\vec{r_i}) + 2\beta_e \sum_i^N b(\vec{r_i}).S_z(i) | \Psi \right\rangle \\ &= \min_{\rho^\alpha, \rho^\beta} \{ \min_{\Psi \to \rho^\alpha, \rho^\beta} \langle \Psi | T + V_{ee} \rangle + \int [v(\vec{r})\rho(\vec{r}) - \int b(\vec{r}) m(\vec{r})] \, d\vec{r} \} \\ &= \min_{\rho^\alpha, \rho^\beta} \{ F[\rho^\alpha, \rho^\beta] + \int \left[(V(\vec{r}) + B_e b(\vec{r})) \rho^\alpha(\vec{r}) + (V(\vec{r}) - B_e b(\vec{r}) \rho^\beta(\vec{r}) \right] d(\vec{r}) \} \end{aligned}$$

Where

$$F[\rho^\alpha, \rho^\beta] = \min_{\Psi \to \rho^\alpha, \rho^\beta} \langle \Psi | T + V_{ee} | \Psi \rangle \tag{3.80}$$

This provides constraint search formulation of the universal functional $F[\rho^\alpha, \rho^\beta]$. The functional $F[\rho^\alpha, \rho^\beta]$ searches all Ψ that yeald the input $\rho^\alpha(\vec{r})$ and $\rho^\beta(\vec{r})$, then $F[\rho^\alpha, \rho^\beta]$ assums the minimum of $\langle T + V_{ee} \rangle$. However $F[\rho^\alpha, \rho^\beta]$ is unknown and approximation is necessary for the theory to be implemented. The Khon Sham method now can be introduced to rigourously handle the kinetic energy contribution to $F[\rho^\alpha, \rho^\beta]$,

$$F[\rho^\alpha, \rho^\beta] = T_s[\rho^\alpha, \rho^\beta] + J[\rho^\alpha + \rho^\beta] + E_{xc}[\rho^\alpha, \rho^\beta] \tag{3.81}$$

Where $T_s[\rho^\alpha, \rho^\beta]$ is the Khon Sham kinetic energy functional corresponding to a system of non interacting electrons with densities ρ^α and ρ^β and $E_{xc}[\rho^\alpha, \rho^\beta]$ is the exchange correlation energy functional. A constrained search definition of T_s can also be given as,

$$T_s[\rho^\alpha, \rho^\beta] = Min \sum_{i\alpha} n_{i\alpha} \int d\vec{r} \, \phi^*_{i\alpha}(\vec{r}) \left(-\frac{1}{2}\nabla^2 \right) \phi_{i\alpha}\vec{r} \tag{3.82}$$

Where the minimization is over the set of $n_{i\alpha}$ and $\phi_{i\alpha}$, with constraints,

$$\sum_i n_{i\alpha} | \phi_{i\alpha}(\vec{r})|^2 = \rho^\alpha(\vec{r}) \tag{3.83}$$

$$\sum_i n_{i\beta} | \phi_{i\beta}(\vec{r})|^2 = \rho^\beta(\vec{r}) \tag{3.84}$$

Suppose the set of $n_{i\alpha}$ and $\phi_{i\alpha}$ minimizes according to the constraint search formula, then we may express the energy as a functionals of the orbitals $\phi_{i\alpha}$

$$E[\rho^{\alpha},\rho^{\beta}] = \sum_{i\alpha} n_{i\alpha} \int d\vec{r}\, \phi^{*}_{i\alpha}(\vec{r}) \left(-\frac{1}{2}\nabla^{2}\right) \phi_{i\alpha}\vec{r} + J\left[\rho^{\alpha}+\rho^{\beta}\right] + E_{xc}[\rho^{\alpha},\rho^{\beta}]$$

$$+ \int [(V(\vec{r}) + B_e b(\vec{r}))\rho^{\alpha}(\vec{r}) + (V(\vec{r}) - B_e b(\vec{r})\rho^{\beta}(\vec{r})]d(\vec{r}) \tag{3.85}$$

The variation search for the minimum of $E[\rho^{\alpha},\rho^{\beta}]$ can then be carried out through orbitals subject to normalization constraints

$$\int \phi^{*}_{i\alpha}(\vec{r})\, \phi_{i\alpha}(\vec{r})\, d(\vec{r}) = 1 \tag{3.86}$$

The resulting Khon-Sham equations are,

$$h^{\alpha}_{eff}\, \phi_{i\alpha}(\vec{r}) = \left[-\frac{1}{2}\vec{\nabla^{2}} + V^{\alpha}_{eff}\vec{r}\right]\, \phi_{i\alpha}(\vec{r}) = \varepsilon_{i\alpha}\, \phi_{i\alpha}(\vec{r}) \tag{3.87}$$

and

$$h^{\beta}_{eff}\, \phi_{j\beta}(\vec{r}) = \left[-\frac{1}{2}\vec{\nabla^{2}} + V^{\beta}_{eff}\vec{r}\right]\, \phi_{j\beta}(\vec{r}) = \varepsilon_{j\beta}\, \phi_{j\beta}(\vec{r}) \tag{3.88}$$

Where the spin dependent effective potentials are

$$v^{\alpha}_{eff}(\vec{r}) = v(\vec{r}) + \int \frac{\rho(\vec{r'})}{|\vec{r}-\vec{r'}|} d(\vec{r}) + \frac{\delta E_{xc}[\rho^{\alpha},\rho^{\beta}]}{\delta\rho^{\alpha}(\vec{r})} + B_e b(\vec{r}) \tag{3.89}$$

$$v^{\beta}_{eff}(\vec{r}) = v(\vec{r}) + \int \frac{\rho(\vec{r'})}{|\vec{r}-\vec{r'}|} d(\vec{r}) + \frac{\delta E_{xc}[\rho^{\alpha},\rho^{\beta}]}{\delta\rho^{\beta}(\vec{r})} - B_e b(\vec{r}) \tag{3.90}$$

In equation 3.89 and 3.90, the number of electrons with α spin and β spin,

$$N^{\alpha} = \int \rho^{\alpha}(\vec{r}) d\vec{r}, \qquad N^{\beta} = \int \rho^{\beta}(\vec{r}) d\vec{r} \tag{3.91}$$

need also to be varried to acheive minimum total energy under the constraint,

$$N = N^{\alpha} + N^{\beta} \tag{3.92}$$

With the spin polarized KS equation, the kinetic energy is handeled exactly and only the exchange correlation energy remains to be determined. The exchange-correlation contribution can be seperated into exchange and correlation pieces,

$$E_{xc}[\rho^{\alpha},\rho^{\beta}] = E_x[\rho^{\alpha},\rho^{\beta}] + E_c[\rho^{\alpha},\rho^{\beta}] \tag{3.93}$$

Where the exchange part is defined as,

$$E_x[\rho^{\alpha},\rho^{\beta}] = -\frac{1}{2}\iint \frac{1}{\vec{r}_{12}}\left\{|\rho_1^{\alpha,\alpha}(\vec{r_1},\vec{r_2})|^2 + |\rho_1^{\beta,\beta}(\vec{r_1},\vec{r_2})|^2\right\}\ d\vec{r}_1 d\vec{r}_2 \tag{3.94}$$

with

$$\rho_1^{\alpha,\alpha}(\vec{r}_1,\vec{r}_2) = \sum_i n_{i\alpha}\ \phi_{i\alpha}(\vec{r}_1)\ \phi^*_{i\alpha}(\vec{r}_2) \tag{3.95}$$

$$\rho_1^{\beta,\beta}(\vec{r}_1,\vec{r}_2) = \sum_i\ n_{i\beta}\ \phi_{i\beta}(\vec{r}_1)\ \phi^*_{i\beta}(\vec{r}_2) \tag{3.96}$$

The $n_{i\alpha}$ and $\phi_{i\alpha}$ are those giving the Khon Sham Kinetic energy, they are determined by ρ^{α} and ρ^{β}.

$$E_x[\rho^{\alpha},\rho^{\beta}] = \frac{1}{2}E_x[\rho^{\alpha},\rho^{\alpha}] + \frac{1}{2}E_x[\rho^{\beta},\rho^{\beta}] \tag{3.97}$$

$$E_x[\rho^{\alpha},\rho^{\beta}] = \frac{1}{2}E_x[\rho^{\alpha},\rho^{\alpha}] + \frac{1}{2}E_x[\rho^{\beta},\rho^{\beta}] \tag{3.98}$$

$$= \frac{1}{2}E_x^0\left[2\rho^{\alpha}\right] + \frac{1}{2}E_x^0\left[2\rho^{\beta}\right] \tag{3.99}$$

where

$$E_x^0[\rho] = E_x\ \left[\frac{1}{2}\rho,\frac{1}{2}\rho\right] \tag{3.100}$$

The Dirac local density approximation for exchange is for the spin compencated case. From above equations, we obtain the local spin density approximation for the exchange energy functionals.

$$E_x^{LSDA}\left[\rho^{\alpha},\rho^{\beta}\right] = 2^{\frac{1}{3}}\ C_x \int \left[(\rho^{\alpha})^{\frac{4}{3}} + (\rho^{\beta})^{\frac{4}{3}}\right]\ d\vec{r} \tag{3.101}$$

Let us define the spin polarization parameter ξ by,

$$\xi = \frac{\rho^{\alpha} - \rho^{\beta}}{\rho} = \frac{\rho^{\alpha} - \rho^{\beta}}{\rho^{\alpha} + \rho^{\beta}} \tag{3.102}$$

Then$\rho^{\alpha} = \frac{1}{2}(1+\xi)\rho$, $\rho^{\beta} = \frac{1}{2}(1-\xi)\rho$ and the LSD exchange energy becomes

$$E_x^{LSD}[\rho^{\alpha}, \rho^{\beta}] = \frac{1}{2}\, C_x \int \rho^{\frac{4}{3}} \left[(1+\xi)^{\frac{4}{3}} + (1-\xi)^{\frac{4}{3}}\right]\, d\vec{r} \tag{3.103}$$

$$= \int \rho \varepsilon_x(\rho, \xi)\, d\vec{r} \tag{3.104}$$

Where

$$\varepsilon_x(\rho, \xi) = \varepsilon_x^0(\rho) + \left[\varepsilon_x^1(\rho) - \varepsilon_x^0(\rho)\right] f(\varepsilon) \tag{3.105}$$

with the exchange density for the spin compensated homogeneous electron gas.

3.6 Generalized Gradient Approximations (GGA)

The LSDA neglects inhonogeneities of real charge density which could be defferent from the Homogeneous Electron Gas (HEG). The exchange correlation energy density has significantly different result from HEG. This gives rise to the various Generalized-Gradient Approximations (GGA) [78] which include density gradient correlation and higher spatial dertiviatives of electron density and gives better result than LDA in many cases. Three most widely used GGA's are the from propeosed by Becke [79], Perdew et al. [80] and Perdew, Burke and Enzerhof [81]. For spin polarized system [82] we know that

$$E_{XC}^{LSDA}\ \ [n_{\uparrow}(r), n_{\downarrow}(r)] = \int n(r)\ \epsilon_{XC}^{hom}\left(n_{\uparrow}(r), n_{\downarrow}(r)\right) dr \tag{3.106}$$

Where, XC energy density $\epsilon_{XC}^{hom}(n(r))$ is a function of the density alone and is decomposed into exchange energy density $\epsilon_X^{hom}(n(r))$ and correlation energy density $\epsilon_C^{hom}(n(r))$. So that the XC energy functional is decomposed into exchange energy functional $E_X^{LDA}[n(r)]$ and correlation energy functional $E_C^{LDA}[n(r)]$ linearly. From

density gradient $\nabla n(r)$,

$$E_{XC}^{GGA} \quad [n_\uparrow(r), n_\downarrow(r)] = \int n(r)\ \epsilon_{XC}^{hom}(n_\uparrow(r), n_\downarrow(r), |\nabla n_\uparrow(r)|, |\nabla n_\downarrow(r)|, ...)dr \quad (3.107)$$

$$= \int n(r)\ \epsilon_X^{hom} n(r))F_{XC}(n_\uparrow(r), n_\downarrow(r), |\nabla n_\uparrow(r)|, |\nabla n_\downarrow(r)|, ...)dr \quad (3.108)$$

Where F_{XC} is dimensionless and $\epsilon_X^{hom} n(r))$ is the exchange energy density of the unpolarized HEG. F_{XC} can be decomposed linearly into exchange contribution F_c as $F_{XC} = F_x + F_c$. Generally GGA works better than LDA, in pridicting binding energy of molecules and bond length, crystal lattice constants, especially the system where charge density varried rapidly. In case of ionic crystall, GGA overcorrects LDA results where the lattice constants of LDA fit well than GGA. But in case of transition metal oxides and rare-earth element, both LDA and GGA parform badly. This drawback leads to approximations beyond LDA and GGA.

Chapter 4

K_2SeCl_6 at ambient pressure

K_2SeCl_6 is a vacancy-ordered double perovskite structure with an alternating arrangement of potassium (K), selenium (Se), and chlorine (Cl) atoms. The vacancy ordering refers to a specific arrangement of these atoms, where vacancies or empty spaces are deliberately created in the crystal lattice. This ordered arrangement of vacancies can trap charge carriers, leading to interesting electronic behavior. Materials with vacancy-ordered double perovskite structures like K_2SeCl_6 are of interest in various technological applications, including solid-state batteries, electronic devices, quantum materials etc.

4.1 Computational details

The physical properties of vacancy-ordered double perovskite K_2SeCl_6 were investigated based on Full Potential Linear Aaugmented Plane Wave (FP-LAPW) method using Density Functional Theory (DFT) as implemented in WIEN2k [45] code. The structural optimization and position minimization for anion were carried out to compute the lattice constants and most stable crystal structure with a space group 225 ($Fm\bar{3}m$). For self-consistant field (SCF) cycle Perdew-Burke-Ernzerhof Generalized-Gradient-Approximation (PBE-GGA) method was used. The limit for charge con-

vergence and energy convergence for the iteration process was set to 10^{-5} Ry and $10^{-4}e$, respectively. The value of the parameter $R_{\mathrm{MT}} \times K_{\mathrm{max}}$, where R_{MT} is the muffin tin radius and K_{max} is the plane wave cut off for reciprocal lattice vector, was set to 8. The maximum values of the Gaussian factor, G_{max} and the angular momentum vector, l_{max} was 16 $(\mathrm{a.u.})^{-1}$ and 10 respectively. The k-mesh was set to 4000 k points in the first Brillouin zone. For mechanical properties, Charpin method was applied while Kramer-Krong model was used to calculate the optical characteristics [90]. Thermoelectric properties were calculated using BoltzTraP [51] code that employs rigid band approximation and classical Boltzman transport theory.

4.2 Structural stability

The crystallographic structure of K_2SeCl_6 is a vacancy-ordered double perovskite containing isolated $[SeCl_6]^{2-}$ octahedrons [91] and ordered vacancies, where K is a monovalent cation, Se is a tetravalent cation and Cl is a halogen anion. The compound crystalizes with the space group 225 ($Fm\bar{3}m$) in a face centered cubic lattice as represented in figure 4.1. The geometrical model contains octahedron of

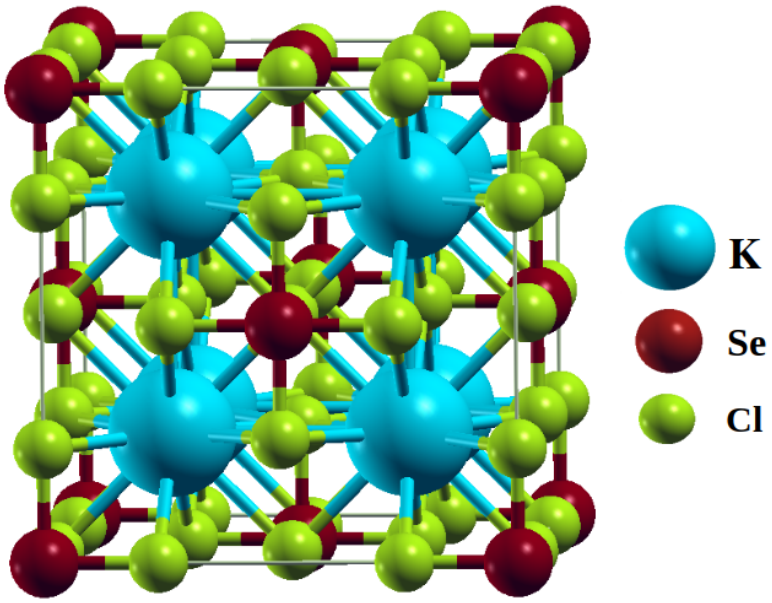

Figure 4.1: Conventional unit cell of vacancy-ordered double perovskite K_2SeCl_6. The light blue color balls signifies the K atoms, the green color balls show the Cl atoms and the red color balls indicate the Se atoms respectively.

$SeCl_6$ with interestitial sites filed by K atoms. Octahedrons are seperated by 12-fold coordinates of Cl atoms. Figure 4.1 shows that K and Se atoms are surronded by 12 and 6 halogen ions respectively. The K, Se, and Cl atoms have 8c Wyckoff sites with (0.25, 0.25, 0.25) coordinates, 4a Wyckoff sites with (0, 0, 0) coordinates and 24e Wyckoff sites with (0.24, 0, 0) coordinates respectively. Volume optimization calculation has been performed to find out the most stable structure with ground state energy of the system. The system exhibits its highest stability with 10.153 Å, demonstrating a notable resemblance to the reference theoretical work [92]. The optimization scheme for total energy in Ry vs volume is represented in figure 4.2. To

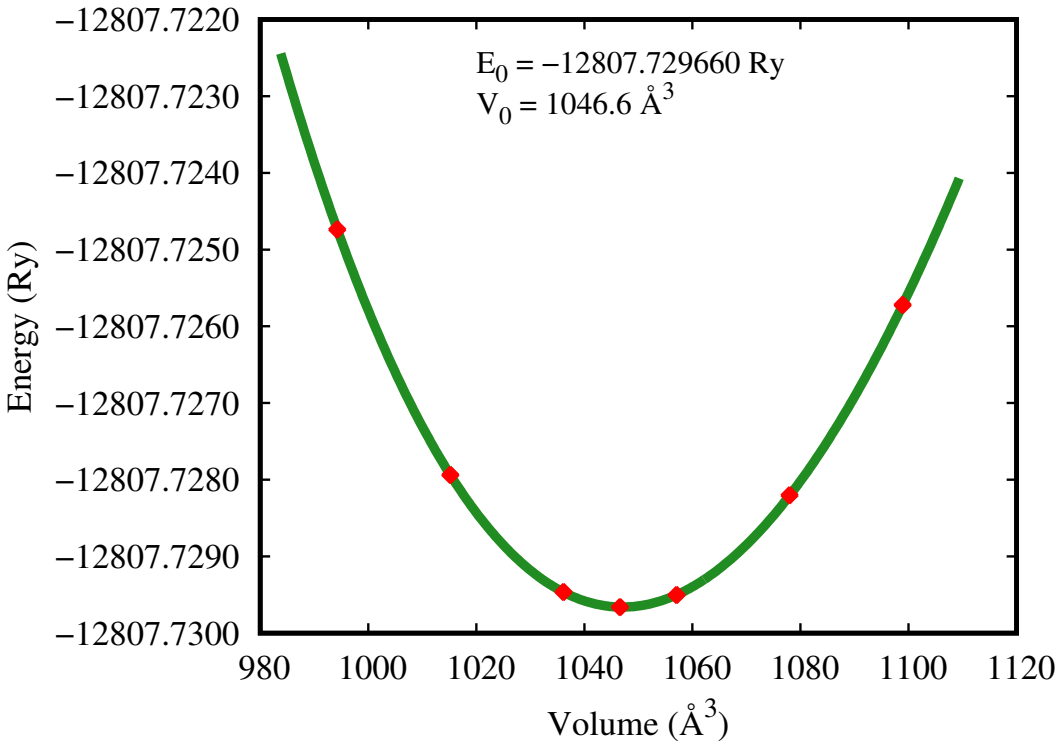

Figure 4.2: Calculated optimized energy vs volume plot of K_2SeCl_6.

evaluate the compound for practical application, structural and thermal stabilities are needed to be investigated. For a perovskite, the ideal value for the Goldsmith tolerance factor which pridicts the stability criteria for a material structure, t_a is 1. However the range from 0.96 to 1.04 is considered to be the best [93]. For K_2SeCl_6,

tolerance factor is found to be 0.98 calculated by the equation [94],

$$t_a = \frac{r_K + r_{Cl}}{\sqrt{2}(r_{Se} + r_{Cl})} \tag{4.1}$$

where r_K, r_{Cl}, and r_{Se} are the ionic radii of K, Cl, and Se respectively. It can be seen that the tolerance factor of K_2SeCl_6 is within the range of perovskite phase stability $0.96 \leq t_a \leq 1.04$ [95] which demonstrates the structural stability of the compound. This fact can be further varified by calculating thermodynamic stability by computing the formation energy, ΔH by the equation [92],

$$\Delta H = E(\mathrm{K_2SeCl_6}) - 2E(\mathrm{K}) - E(\mathrm{Se}) - 6E(\mathrm{Cl}) \tag{4.2}$$

Where ΔH is the formation energy, $E(\mathrm{K_2SeCl_6})$ is the total energy of the system, E(K), E(Se), and E(Cl) are the total energies of K, Se, and Cl atoms respectively. For K_2SeCl_6, formation energy is found to be -0.53 eV. The negative formation energy indicates the thermodynamic stability of the compound.

4.3 Electronic properties

In order to determine the probable region for practical applications of the studied compound, analysis of band structure and density of states is regarded to be essential. To verify the band gap dependent properties and intra band transitions, the bandstructure, total and partial density of states are calculated and plotted in figure 4.3 to 4.5. Bandstructure shows, K_2SeCl_6 is a p type semiconducting material with an indirect band gap of 2.502 eV. The valence band maxima is at W and conduction band minima is at L as can be seen from figure 4.3. Bandstructure is plotted along with high symmetry points in the first Brillouin zone. Semiconductors having bandgap greater than 2 eV is called wide band gap semiconductor [96]. It is evident that compound K_2SeCl_6 is a wide band gap semiconductor having great potential in optoelectronic applications. In bandstructure, the more states are present at the valence band edge (much closer to the Fermi level than the conduction band) which occurs due to comparatively large holes effective masses as compared to the elec-

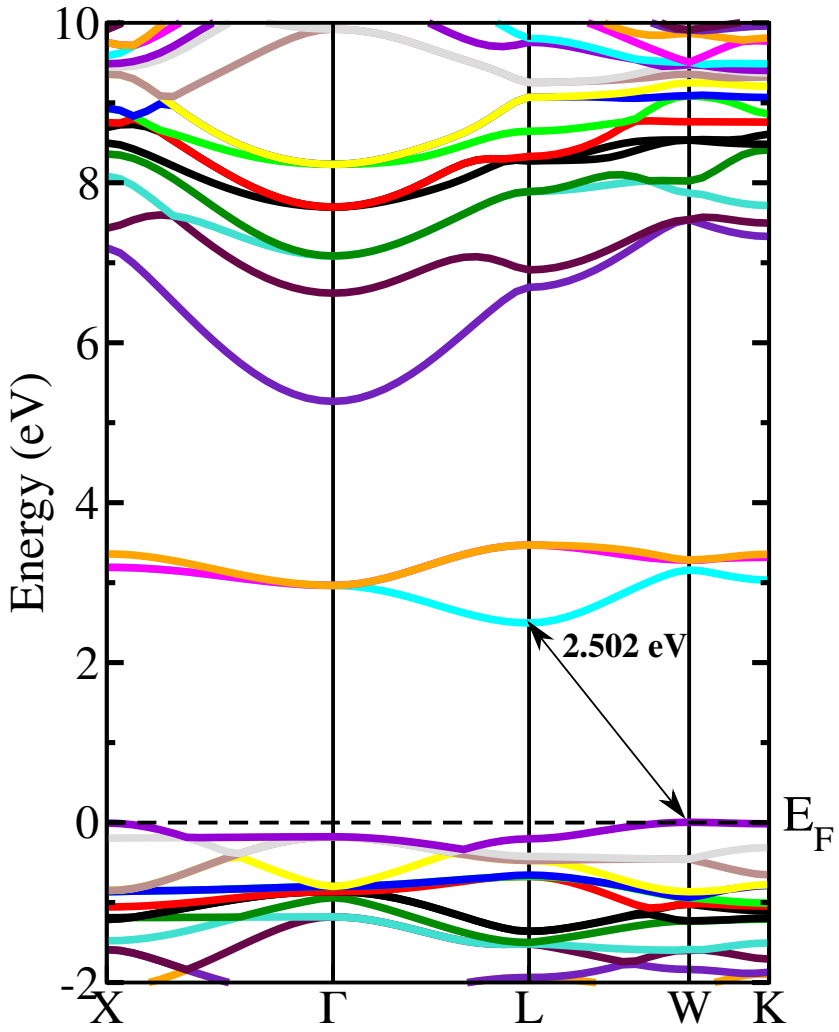

Figure 4.3: The calculated bandstructure using PBE approximation for K_2SeCl_6 at ambient pressure.

trons. To understand the possible electronic transition from valence to conduction band and hybridization among the constituent states, the total and partial density of states are computed as shown in figure 4.4 and 4.5. The total and partial DOS shows the total contribution of individual atoms and states in valence and conduction band which is equivalent to the band structure. The individual K, Se, and Cl atoms have electronic configuration as $[Ar]4s^1$, $[Ar]3d^{10}4s^24p^4$, and $[Ne]3s^23p^5$ respectively. For hybridization and inter-band transitions, only the valence electrons are responsible. It is evident from figure 4.4 (a) that the valence band near the fermi level mostly originated by Cl 3p states with a small contribution of Se 4p states (figure 4.5a).

The conduction band minimum also originated by Cl 3p and Se 4p states. The energy bands above 5.27 eV (figure 4.4b) is mainly because of hybridized K 4s states which can have a significant influence on the exibited physical properties. But only the states composing the valence band maxima and conduction band minima are responsible to originate the physical properties of a compound.

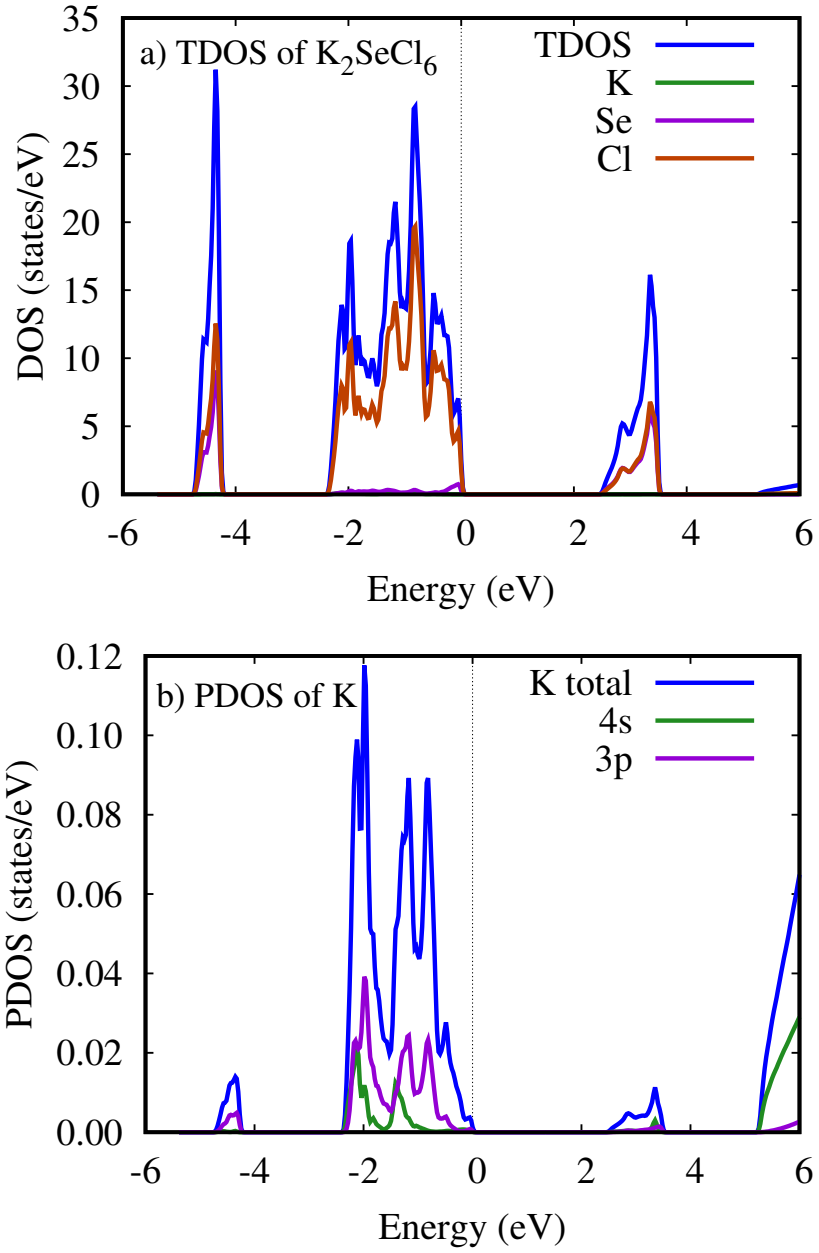

Figure 4.4: a) Total density of states of K_2SeCl_6, b) Partial density of states of K at ambient condition.

So it can be said that for our computed system, the possible indirect transition can be resulted from Cl 3p from valance band to Cl 3p and Se 4p in conduction band. Therefore, the p-p hybridizations are responsible for excitation and recombination for our system.

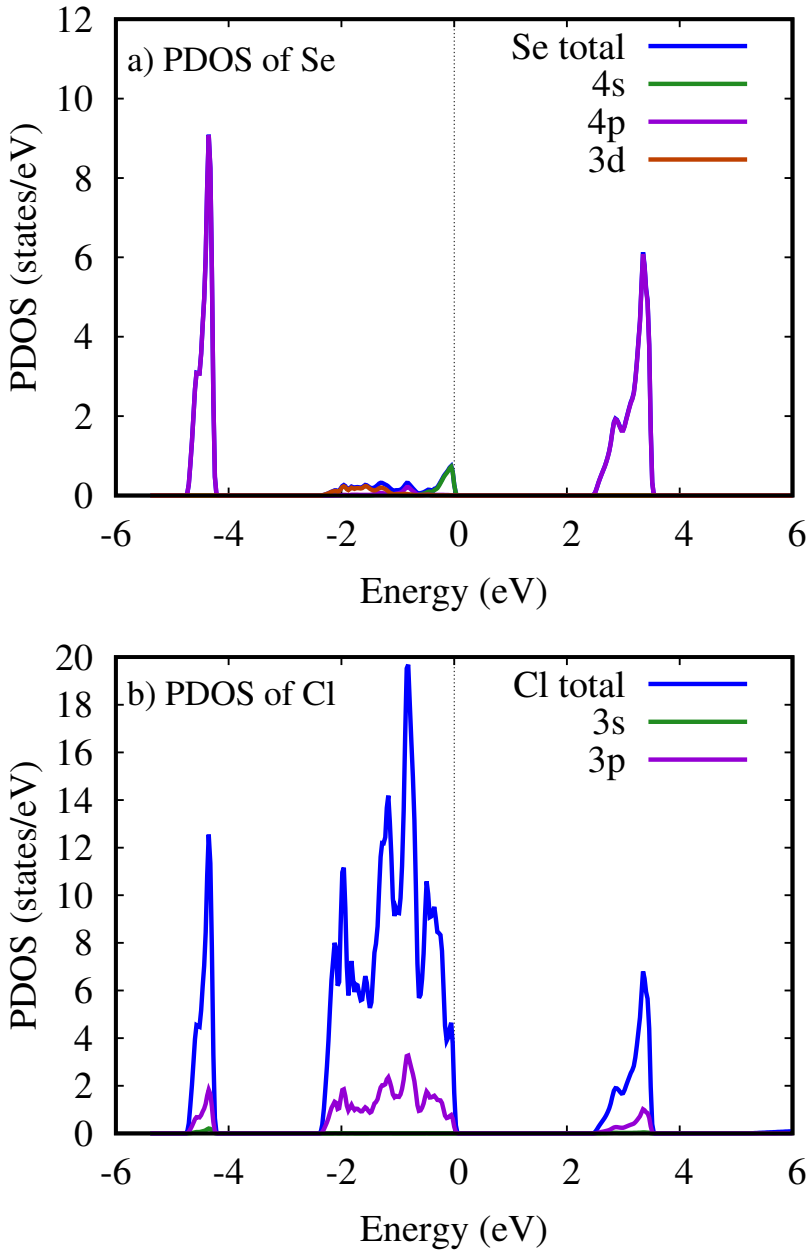

Figure 4.5: a) Partial density of states of Se and b) Partial density of states of Cl at ambient condition.

4.4 Optical properties

The indirect band gap semiconducting property of K_2SeCl_6 reveals its potential for optoelectronic and solar cell applications in visible region [97]. The optical properties of K_2SeCl_6 at ambient pressure were calculated and plotted in figure 4.6-4.8 to understand the nature of light-matter interaction in that system. The electromagnetic resonance between the incident light and the bound electrons in the valence band has an impact on the optical response. When energy is encountered, the bound electrons absorb it and move into the conduction band and the process of recombination is used to evaluate a material's potential for optoelectronic applications [98,99]. In this study, we elaborated the complex dielectric function $\varepsilon(\omega)$, absorption coefficient $\alpha(\omega)$, optical conductivity $\sigma(\omega)$, reflectivity $R(\omega)$, and refractive index $n(\omega)$ to understand band gap-dependent optical features of the compound. The complex dielectric function can be calculated by the equation,

$$\varepsilon(\omega) = \varepsilon_1(\omega) + i\varepsilon_2(\omega) \tag{4.3}$$

Where, $\varepsilon_1(\omega)$ and $\varepsilon_2(\omega)$ are the real and imaginary part of the dielectric function. The real part explains the degree of polarization of a compound as a response to electromagnetic wave interactions whereas the imaginary part indicates loss factor or the absorption of incident light energy. The static values of $\varepsilon_1(\omega)$ are related with the threshold for optical absorption according to Penn's model [100] that can be represented by

$$\varepsilon_1(0) \approx 1 + (\hbar\omega_p/E_g)^2 \tag{4.4}$$

Here, ω_p and $\hbar$ are plasma frequency and reduced Plank's constant respectively. The values of $\varepsilon_1(\omega)$ and $\varepsilon_2(\omega)$ for the compound K_2SeCl_6 are plotted in figure 4.6. In figure 4.6 (a), $\varepsilon_1(\omega)$ increases by increasing photon energy and become highest at 3 eV. This peak predicts that the studied compound is fully polarized and at energy 5 eV, the negative value of $\varepsilon_1(\omega)$ expresses the typical semiconducting nature in visible region and changed to metallic after 5 eV in Ultra Violet region.

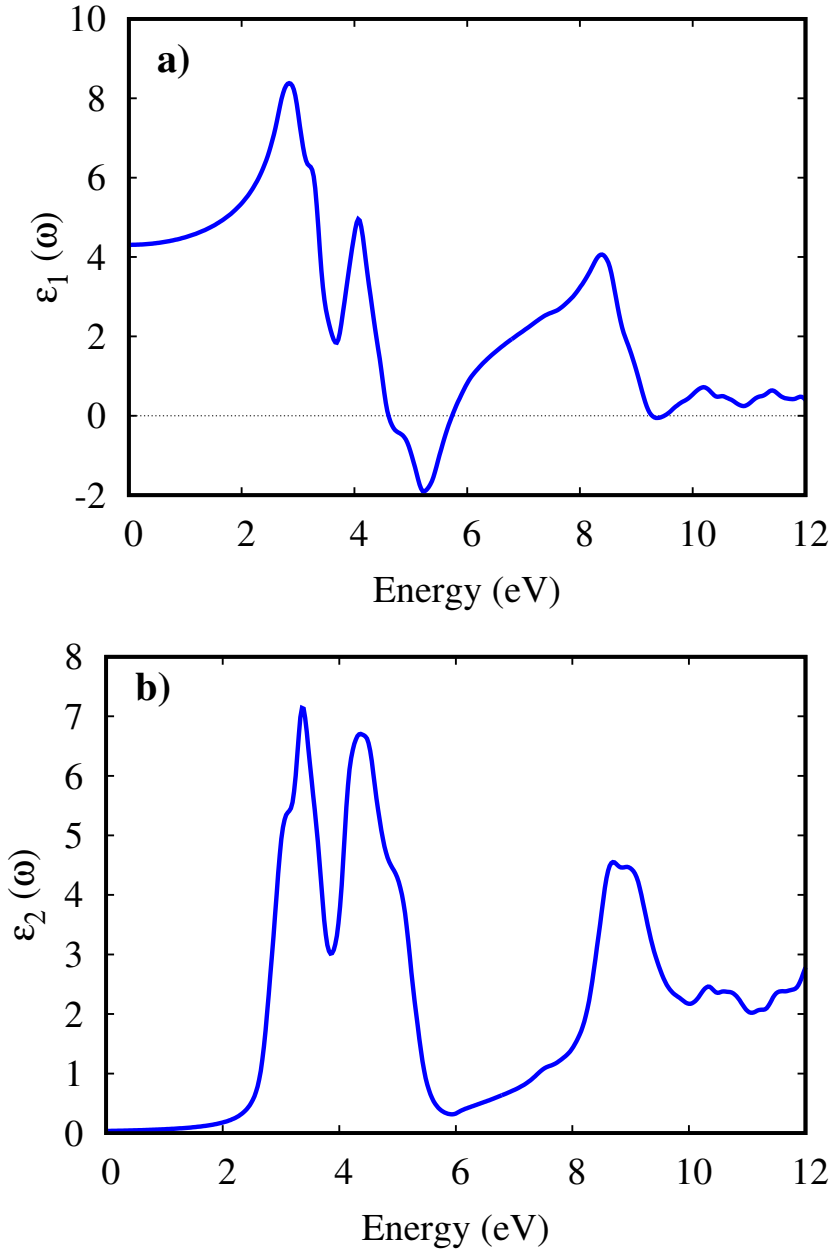

Figure 4.6: The computed optical parameters a) Real dielectric function and b) Imaginary dielectric function of K_2SeCl_6 at ambient condition.

The $\varepsilon_1(\omega)$ and $\varepsilon_2(\omega)$ are related through Kramer-Kroning relation [101]

$$\varepsilon_1(\omega) = 1 + \frac{2}{\pi} P \int_0^\infty \frac{\omega' \varepsilon_2(\omega')}{\omega'^2 - \omega^2} \tag{4.5}$$

$$\varepsilon_2(\omega) = \frac{e^2 h}{\pi m^2 \omega^2} \sum_{v,c} \int_{BZ}^\infty |M_{cv}(k)|^2 \, \delta[\omega_{cv}(k) - \omega] d^3k \tag{4.6}$$

where P and k shows the principle quantum number and wave vector respectively. The h is a Plank constant, ω is the angular frequency, and M is the molar mass of the carriers.

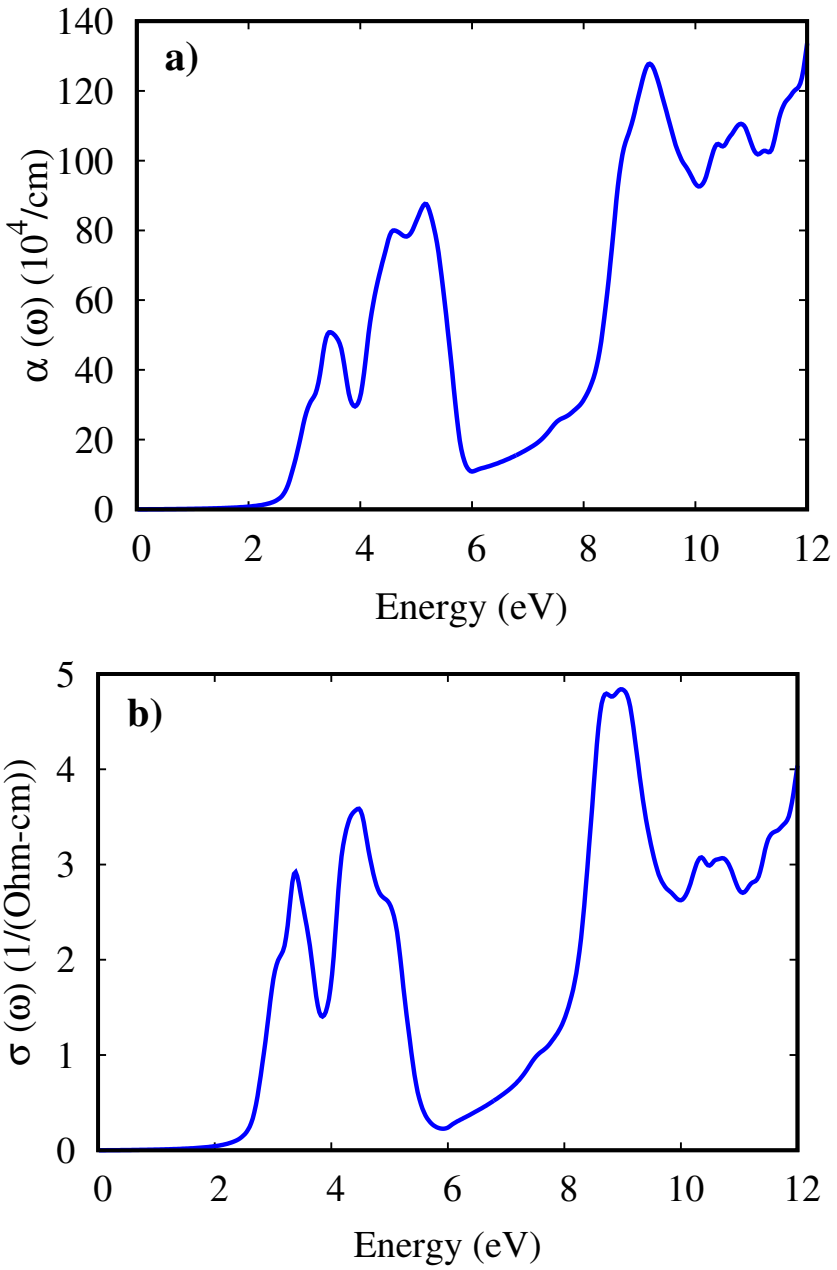

Figure 4.7: a) Absorption coefficient and b) Optical conductivity of K_2SeCl_6 at ambient condition.

The imaginary dielectric function shows the light absorption probability of the compound when a light of suitable energy falls on it. Threshold value of light absorption

is proportional to the optical band gap and after this threshold energy, absorption of light starts. For K_2SeCl_6, this threshold is 2.502 eV as can be seen from figure 4.6 (b) which agree to the electronic band gap extracted from band structure. The value of $\varepsilon_2(\omega)$ reaches to a maximum at the boundary of visible region ranging from 3 to 4 eV.

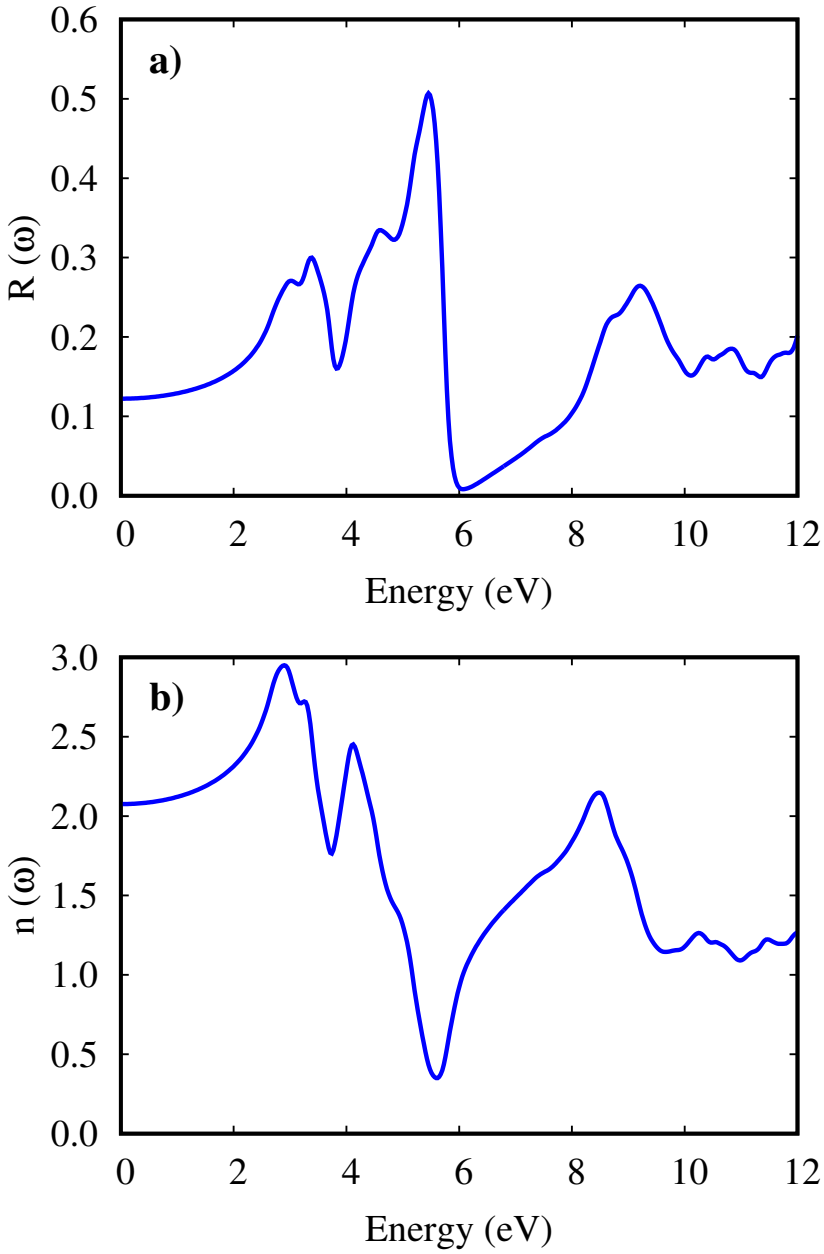

Figure 4.8: a) Optical reflectivity and b) Refractive index of K_2SeCl_6 at ambient condition.

The second peak occurs at energy 4.5 eV in ultraviolet region. The absorption

coefficient $\alpha(\omega)$ also measures the light absorption incident on the studied material as plotted in figure 4.7 (a). $\alpha(\omega)$ can be calculated by the following equation,

$$\alpha(\omega) = \sqrt{2}\frac{\omega}{c}\{\sqrt{\varepsilon_1^2(\omega) + \varepsilon_2^2(\omega)} - \varepsilon_1(\omega)\}^{\frac{1}{2}} \tag{4.7}$$

The incident energy below the bandgap can not cause any electronic transition from valence band to conduction band. The extracted absorption edge 2.5 eV for the compound K_2SeCl_6 is found consistent with the electronic band gap. Both absorption coefficient and imaginary dielectric constant are analogous to each other since both explains absorption of light. After threshold, as photon energy increases, $\alpha(\omega)$ reaches its first peak at 3.5 eV and second peak at 5 eV. After 5 eV, absorption coefficient starts decreasing with further increase in photon energy. The electrical conductivity $\sigma(\omega)$ in figure 4.7 (b) illustrates the optical current generated due to liberated free carriers as a result of incident energy. The incident photon energy excites valence electrons to move to the conduction band which determines the electical or optical conductivity of the compound. The first peak in optical conductivity occurs at 3.5 eV and second peak at 4.5 eV which is analogous to the absorption coefficient. When light falls on a material, absorption, reflection and transmission occurs simultaneously. For inventigating the reflected light from the surface, reflection coefficient $R(\omega)$ can be computed by the equation,

$$R(\omega) = \frac{-i\omega\,(\varepsilon_2(\omega) - 1)}{4\pi} \tag{4.8}$$

For K_2SeCl_6, optical reflectivity has been calculated and plotted in figure 4.5 (e). With the increment of photon energy, reflectivity increases and becomes maximum (50%) at 5 eV. At visible region maximum reflectivity is 30%. Such a small value of $R(\omega)$ is considered to have a small influence on the performance of practical devices. The refractive index $n(\omega)$, sensitive to the wavelength, group velocity and nature of the material expresses the energy dispertion of the materials is analogous to the real dielectric function of the material is also calculated and plotted against the photon energy in figure 4.8 (b). The computed $n(\omega)$ exibits maxima at 3 eV and minima at 5.5 eV for the studied compound. Refractive index $n(\omega)$ and $\varepsilon_1(\omega)$ are related to

each other according to the expression $n^2 - k^2 = \varepsilon_1(\omega)$. Therefore zero frequency values of the refractive index and real dielectric constant $\varepsilon_1(0)$ satisfy the equation $n_0^2 = 0$. However the optical properties of K_2SeCl_6 at ambient pressure reveals that the compound has the potential for the optical device application in the visible and ultra violet region.

4.5 Thermoelectric properties

In order to explore the electric transport behavior, it is important to understand the thermoelectric properties of various substances. Thermoelectric materials have been thoroughly studied for energy harvesting applications in the last few decades [102]. Several important characteristics, such as temperature-dependent electrical conduction, can be used to analyze the performance of any thermoelectric material with a certain band gap [103]. The thermoelectric properties of K_2SeCl_6 has been examined by calculating electrical conductivity (σ/τ), seebeck coefficient (S), thermal conductivity (κ_e/τ), power factor (PF = $\sigma S^2/\tau$), and figure of merit (ZT = $\sigma S^2/\kappa\tau$) [104] as plotted in figure 4.9 to 4.11. Here τ is the relaxation time, which for a typical semiconductor has a constant value with an order of 10^{-14} s. For our computed system, no experimental measurement of τ has been found. In a compound, the flow of charge through the material can be measured by the electrical conductivity. For an effective thermoelectric device, materials should have high electrical conductivity to minimise the Joule heating effect [105]. The computed electrical conductivity per relaxation time (σ/τ) for K_2SeCl_6 is represented in figure 4.9 (a) as a function of the temperature ranges from 100K to 1000K. Since a number of variables, including charge carrier concentration, charge magnitude, and mobility affect electrical conductivity, figure shows the conductivity of the compound increases linearly with temperature, which signifies an increase in the carrier concentration associated with electrical conduction. From figure, breaking bonds and creating electron hole pairs with enough energy to significantly contribute to electrical conduction is possible even at 100K. The increase in electrical conductivity expresses continuously increasing carrier concentration, which indicates a negative temperature coefficient of

resistivity, is demonstrated and supports the examined compound's semiconductor nature.

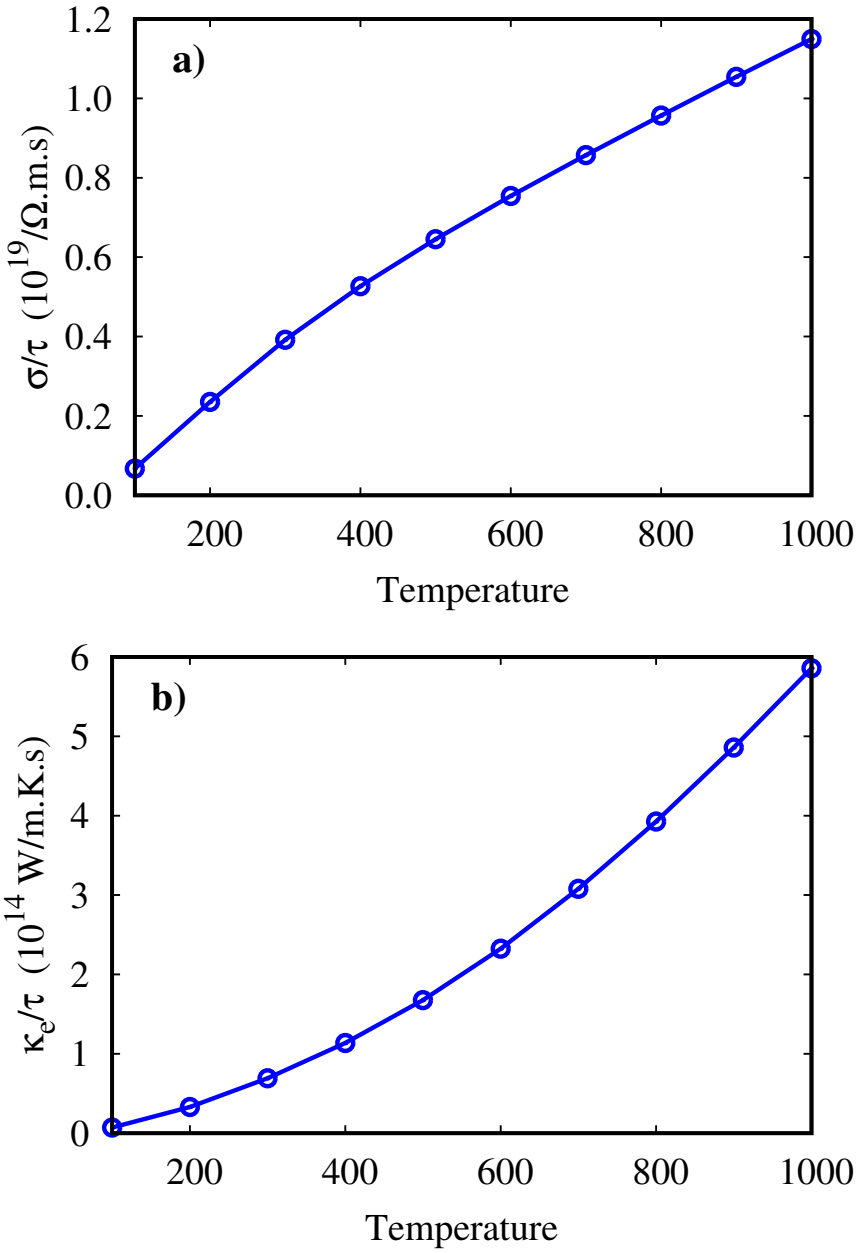

Figure 4.9: The calculated a) Electrical conductivity (σ/τ) and b) Thermal conductivity (k_e/τ) for K_2SeCl_6 at ambient condition as a function of temperature (T).

At 100K, K_2SeCl_6 has a minimum value of σ/τ, which indicates its suppressed charge carriers mobility that may be related to its wide band gap. The thermal conductivity κ_e/τ in figure 4.9(b) exhibits a similar pattern as for σ/τ results from increasing temperature that enhances the kinetic energy of the carriers. For any

thermoelectric material, an optimized value of electronic and thermal conductivities is required to exhibit higher thermoelectric efficiency.

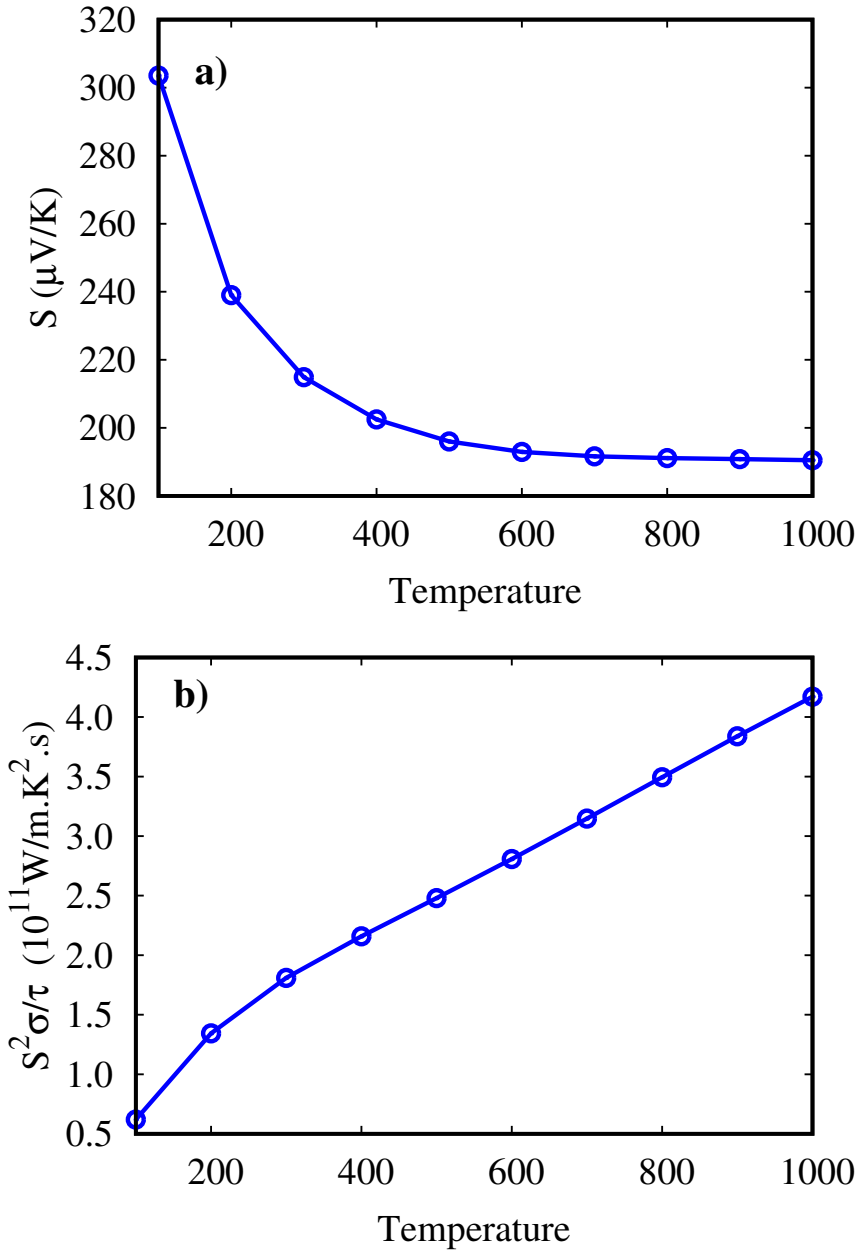

Figure 4.10: The calculated a) Seebeck coefficient (S) and b) Power factor (PF) of K_2SeCl_6 at ambient condition as a function of temperature (T).

The κ/τ has electronic κ_e/τ and lattice κ_l/τ contributions respectively. Here we have elaborated κ_e/τ only. For illustration of performance, from the Wideman Franz law κ_e/σ factor having value in the range 10^{-6} ensure the comparative contribution of

σ/τ is more than κ_e/τ. For our system, κ_e/τ improves from 0 to 6×10^{14} W/mKs at 1000K. Seebeck coefficient (S) determines the ability of a material to generate the electromotive force from the applied temperature gradient through the material, in other word, it indicates the effectiveness of the thermocouples [106]. The electronic movement causes thermoelectromotive force which produces voltage in microvolt per kelvin.

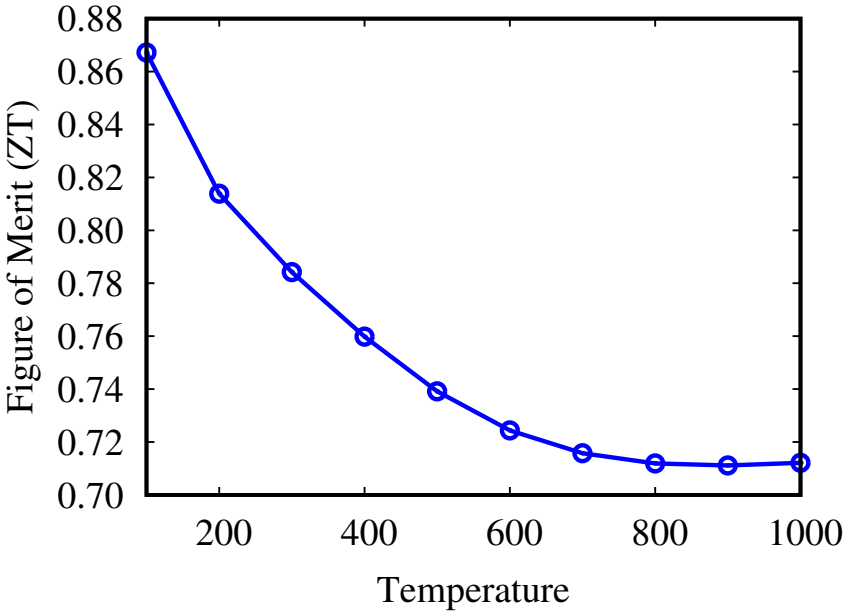

Figure 4.11: Calculated Figure of Merit (ZT) of K_2SeCl_6 at ambient condition as a function of temperature (T).

For better thermoelectric efficiency, we need the large value of Seebeck coefficient (S). Seebeck coefficient can be eleborated by the Piserenko relation [107, 108]

$$S = 8\pi^2 k_B m^* T (3eh^2)^{-1} (\frac{\pi}{3\rho})^{\frac{2}{3}} \tag{4.9}$$

Where, k_B shows Boltzman constant, m^* is the effective mass, e is charge carriers, h is Plank's constant, ρ express carriers concentration and T represents absolute temperature. In figure 4.10 (a), Seebeck decreases from 300 μV/K to 190 μV/K at 1000K temperature. Because in this temperature range, increasing σ/τ decreases the potential barrier. The value of S $\geq$ 200 μV/K are indicative of the excillent thermoelectric materials [109]. In our calculation, 214 μV/K is found for the seebeck

Table 4.1: The depicted values of Electrical conductivity (σ/τ), Thermal conductivity (κ_e/τ), Seeback coefficient (S), Power factor (PF), and Figure of Merit (ZT) for K_2SeCl_6 at ambient pressure and room temperature (300 K).

Specification	σ/τ ($\times 10^{19}\Omega$ms)	k_e/τ ($\times 10^{14}$W/mK)	S (μV)/K	PF ($\times 10^{11}$ W/mK^{2}s)	ZT
K_2SeCl_6	0.391	0.692	214	1.809	0.784

coeeficient at room temperature which is remarkably outstanding to the mentioned value. Therefore the studied double perovskite material has excillent potential for thermoelectric application. The efficiency of a thermoelectric material without including thermal conductivity can be explained using power factor (PF = $\sigma S^2/\tau$) that increases from 0.6 to 4.2$\times 10^{11}$ W/mK^{2}s at 1000K temperature (figure 4.10 b). For a more accurate evaluation of the thermal to electrical energy conversion, the figure of merit (ZT = $\sigma S^2/\kappa\tau$) also determined and plotted in figure 4.11 for the temperature ranges from 0 to 1000K. At 100K ZT is 0.87 for K_2SeCl_6 and decreases with temperature and exhibit 0.784 at 300K temperature. With further increment of temperature, ZT decreases gradually. Therefore, at room temperature and ambient pressure K_2SeCl_6 appears to be a relatively useful thermoelectric material for practical applications.

Chapter 5

Pressure dependent characteristics of K_2SeCl_6

Pressure dependent studies reveals emergent phenomena, such as differences in optoelectronic and thermoelectric properties of a compound, that are not present under ambient conditions. Pressure can enhance or suppress charge carrier mobility, modify the activation energy for conduction, and induce changes in the thermoelectric properties. Pressure dependent investigations provide insights into the charge transport mechanisms and enable the design of materials with improved conductivity under specific pressure conditions [110]. It offers chances to design and enhance material properties for certain technological uses. Understanding and harnessing these emergent phenomena under pressure can lead to the discovery of unique physical properties and potential applications of a material.

5.1 Electronic properties

The impact of pressure on the electronic properties of a compound manifests as alterations in its behavior under high-pressure conditions. These changes can significantly affect electronic structure, band gap, conductivity, and other pertinent

properties of the material. High pressure often prompts shifts in interatomic distances and lattice parameters, thereby inducing modifications in the electronic band structure. Additionally, the application of high pressure can lead to phase transitions or adjustments in the density of states within the electronic structure. Under ambient conditions, the most stable configuration of K_2SeCl_6 is found with a lattice parameter of 10.153 Å, demonstrating an indirect band gap of 2.502 eV.

Table 5.1: The obtained values of lattice parameter (Å) and band gap (eV) for K_2SeCl_6 under all applied pressures.

Pressure (GPa)	Lattice Parameter (Å)	Band Gap (eV)
0	10.153	2.502
5	9.737	2.545
10	9.486	2.508
20	9.168	2.307
40	8.805	2.067
60	8.582	1.799
80	8.423	1.568

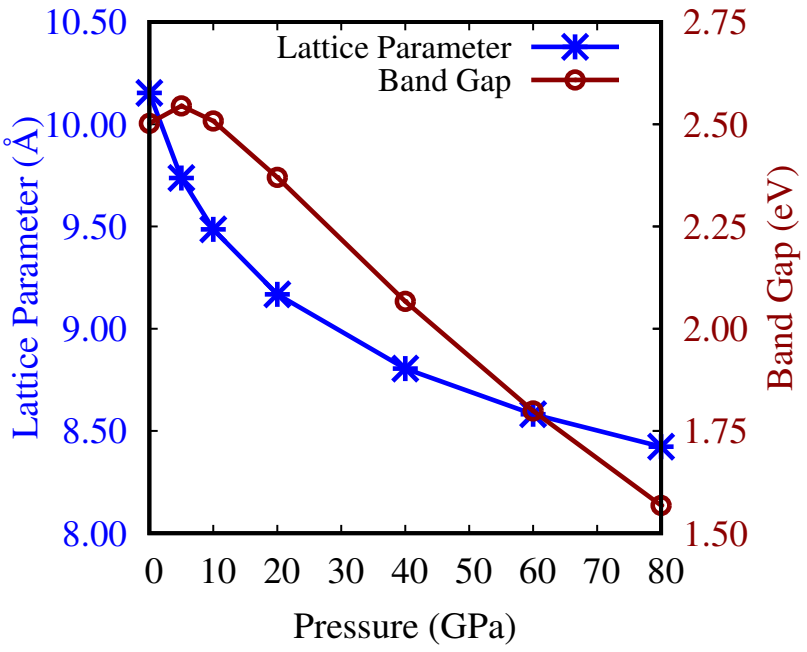

Figure 5.1: The reduction of lattice parameter and band gap of K_2SeCl_6 in response to the applied pressure.

Under applied pressure, both the lattice parameter and band gap undergo a gradual decrease. At 80 GPa, the band gap decreases to the point where it approaches the boundary of the visible energy region.

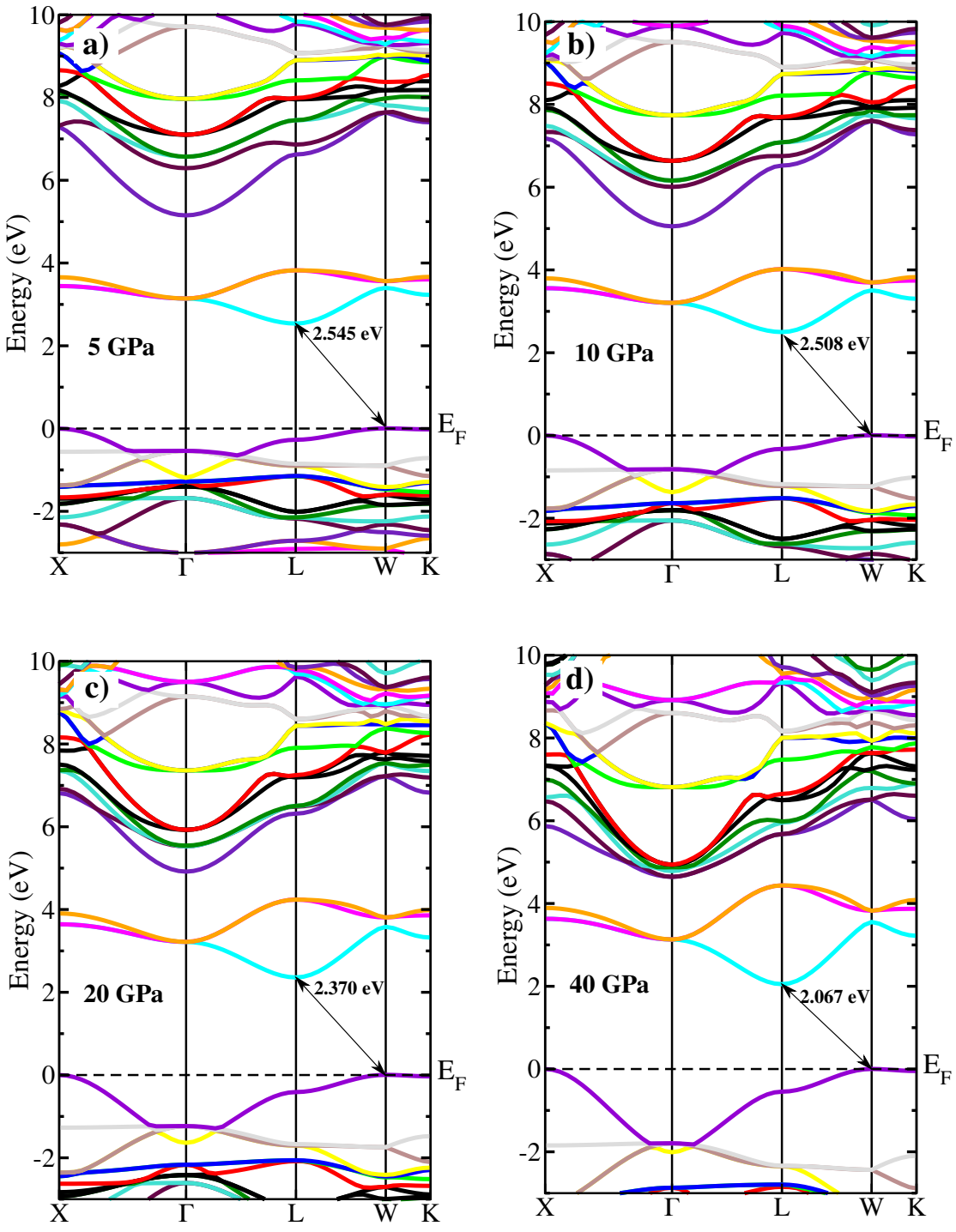

Figure 5.2: The calculated band structures of vacancy-ordered double perovskite K_2SeCl_6 under applied pressures ranging from 5 to 40 GPa.

Figure 5.1 illustrates the reduction in lattice parameter and band gap as pressure is applied, while Table 5.1 provides specific values for the lattice parameter and band gap corresponding to each applied pressure. In order to verify the changes in electronic properties induced by pressure, we performed computations for the band structure, total, and partial density of states for K_2SeCl_6 up to 80 GPa, comparing the results with the ambient condition, as shown in Figures 5.2 to 5.4. In Figures 5.2 and 5.3, the horizontal dotted line at 0 eV represents the Fermi level for all. At 0 GPa, K_2SeCl_6 exhibits an indirect band gap of 2.502 eV with a p-type semiconducting nature. At 5 and 10 GPa, the band gap increased by 0.043 and 0.006 eV,

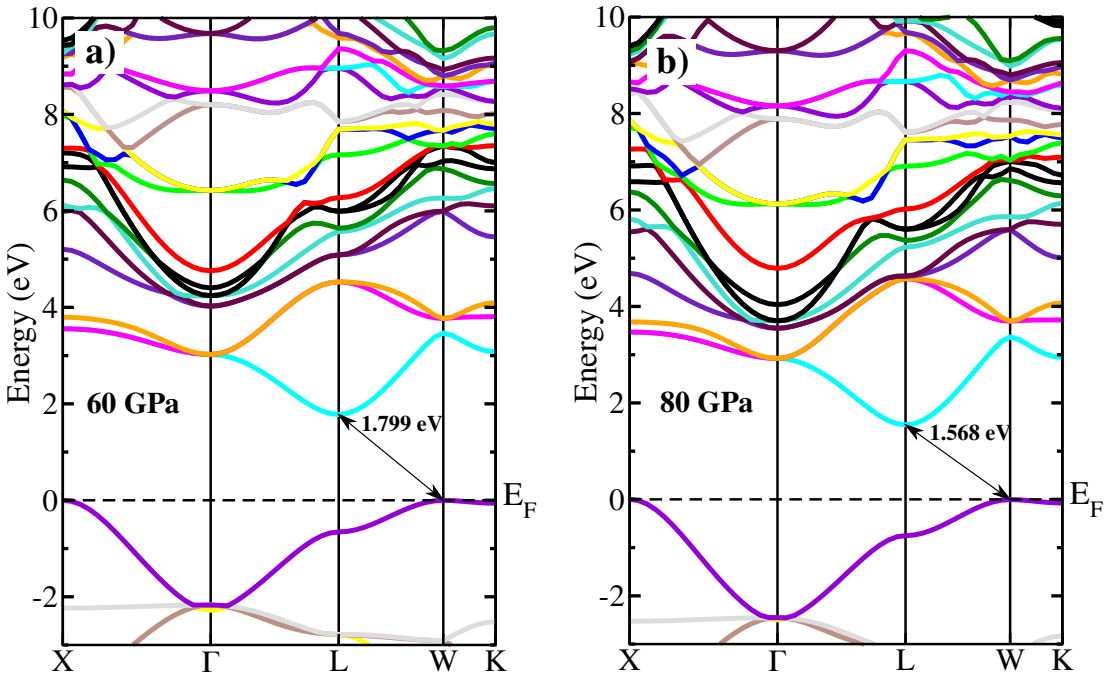

Figure 5.3: The calculated band structures of the double perovskite K_2SeCl_6 under applied pressures of a) 60 GPa and b) 80 GPa show a gradual decrease in the band gap compared to ambient conditions as the applied pressure increases.

respectively, compared to 0 GPa. Beyond 20 GPa, there is an observed inverse relationship between the band gap and external pressure [111]. This relationship may intensify the potential between electrons and ions, contributing to a reduction in the lattice parameter. As pressure continues to rise, the conduction band minimum progressively approaches the Fermi level, leading to a decrease in the band gap. The reduced gap facilitates easier movement of electrons from the valence band to the

conduction band. This is evident in Figures 5.2 and 5.3, where an increase in induced pressure correlates with a rise in the density of bands in the conduction region and a gradual decrease in the valence band. Furthermore, the bands of K migrate towards the conduction band, contributing to the reduction of the gap between 4 to 5 eV. Around 60 GPa, this gap completely vanishes due to the influence of energy bands associated with K.

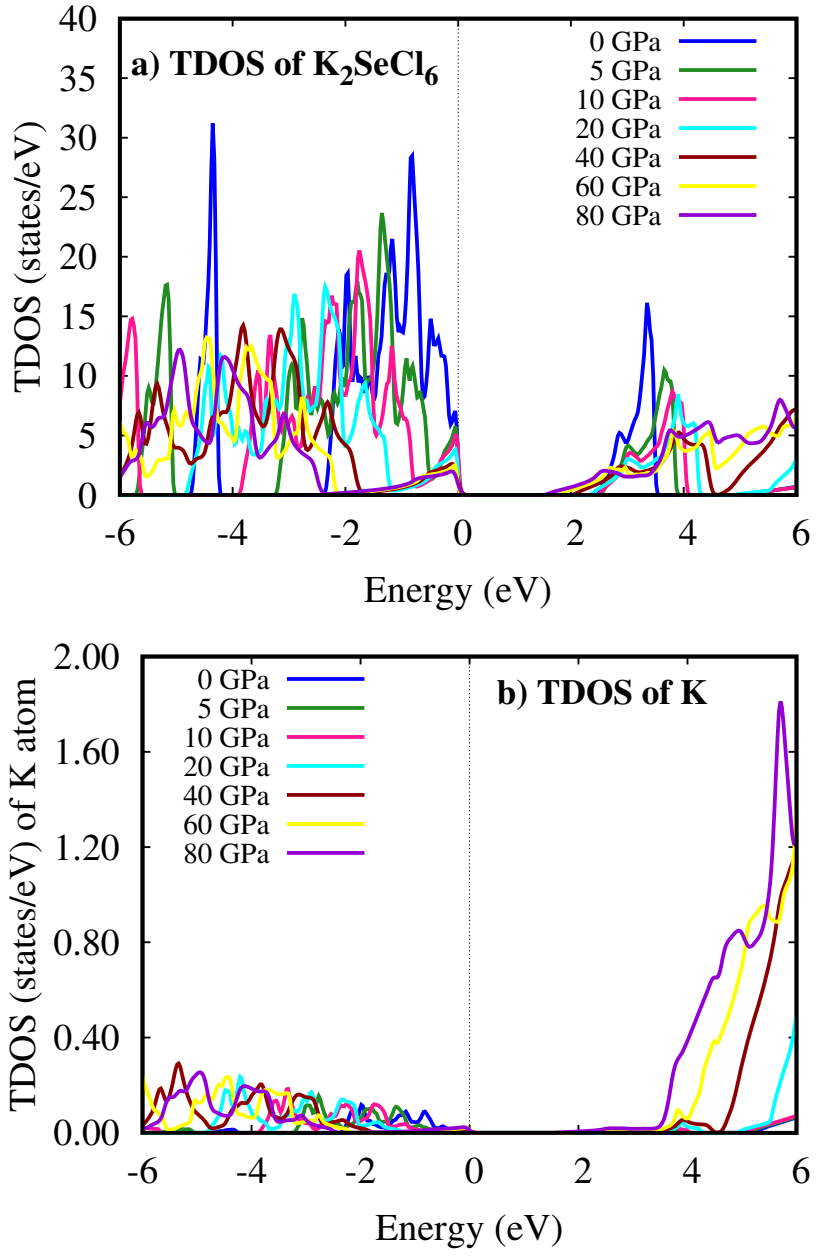

Figure 5.4: The calculated a) Total density of states and b) Total density of K atoms for K_2SeCl_6 upto 80 GPa compared to ambient condition.

Consequently, it can be affirmed that as pressure increases, a growing number of electrons transition from the valence to the conduction bands, thereby enhancing conductivity and other optoelectronic properties. These enhanced properties make the material more favorable for various device applications. For a more detailed explanation of the band structure, the total density of states (TDOS) for K_2SeCl_6 under all applied pressures has been computed and is illustrated in Figure 5.4 (a), with a comparison to the 0 GPa condition.

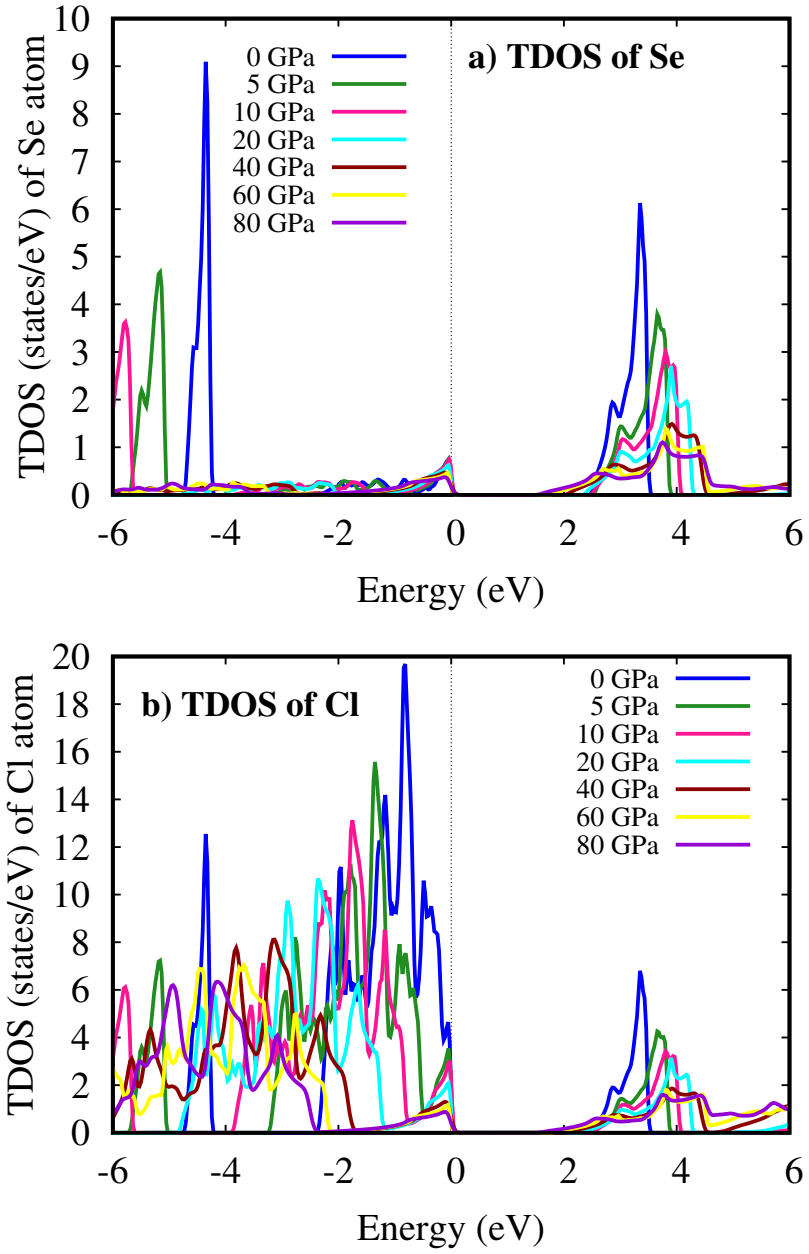

Figure 5.5: The calculated a) Total density of states of Se atom and b) Total density of states of Cl atom for K_2SeCl_6 upto 80 GPa compared to ambient condition.

It's noteworthy that K_2SeCl_6 maintains its p-type semiconducting nature under all applied pressures, consistent with its behavior at 0 GPa. The sharp peaks in the TDOS, when subjected to pressure, gradually shift downward, signifying a substantial influence of pressure on the total density of states. The band gap undergoes a reduction under pressure due to the shift in this peak, as observed in the band structures also. Figures 5.4 (b) and 5.5 represent the computed total densities of states for K, Se, and Cl. This is done to elucidate potential band transitions from valence to the conduction region and to highlight recombination among the constituent states. It is noteworthy that only valence electrons participate in inter-band transitions and hybridization. The total density plot of K, Se, and Cl makes it clear that the valence band, particularly near the Fermi level, is primarily derived from Cl 3p states, with a minor contribution from Se 4p states. Similarly, the conduction band minimum is also predominantly influenced by Cl 3p and Se 4p states. In Figure 5.4 (b), with increasing pressure, the K 4s orbitals within the conduction band shift downward, forming a distinct peak between 2.502 to 4 eV energy bands, and exhibit a sharp peak at 5 to 6 eV for 80 GPa. Figure 5.5 (a) illustrates the Total Density of States (TDOS) for Se, indicating that the Se 4p orbital has a noteworthy contribution to the lower valence energy region under ambient conditions. However, as pressure rises, this contribution gradually diminishes both in the valence and conduction bands. The gap between 4 to 5 eV experiences a gradual filling, primarily by a substantial contribution from K 4s orbitals, accompanied by a minor presence of Cl 3p and Se 4p. As pressure increases, the Se 4p and Cl 3p orbitals descend, leading to a reduction in the band gap of K_2SeCl_6. Consequently, the band gap decreases from 2.502 eV to 1.568 eV under an applied pressure of 80 GPa.

5.2 Mechanical properties

Mechanical properties play a significant role in the engineering of materials for industrial use. This property can be elaborated by tension analysis by the non-linear differential equation by Charpin method. Properties include second order elastic constants (C_{ij}), Bulk modulus, Young's modulus, Shear modulus, Poisson's ratio,

Table 5.2: Calculated C_{11}, C_{12}, C_{44}, Bulk modulus (B), Shear modulus (G), Young's modulus (E), Pugh's ratio (B/G), Poisson's ratio (ν), Cauchy pressure, Elastic anaisotropy (A) and Debye temperature (θ_D) of K_2SeCl_6 at different hydrostatic pressure.

Specifications	Pressure (GPa)						
	0	5	10	20	40	60	80
C_{11}(GPa)	54.840	101.322	132.398	183.509	269.115	328.997	318.360
C_{12}(GPa)	13.803	19.292	24.645	33.313	46.864	57.674	68.003
C_{44}(GPa)	12.969	16.815	17.085	21.371	34.973	41.411	47.296
B (GPa)	27.482	46.635	60.562	83.378	120.947	148.114	172.455
G(GPa)	15.207	24.251	27.653	36.400	56.807	68.228	78.334
E(GPa)	38.512	62.005	72.000	95.327	147.351	177.438	204.099
B/G	1.762	1.923	2.190	2.291	2.129	2.171	2.202
ν	0.270	0.278	0.301	0.309	0.296	0.300	0.302
$C_{12} - C_{44}$	0.834	2.477	7.569	11.942	11.891	16.263	20.707
A	0.145	0.411	0.317	0.284	0.315	0.305	0.301
θ_D (K)	277.483	339.521	358.887	405.175	495.275	536.115	596.256

ductility, brittleness, anisotropy, elastic wave propagation, and other solid state phenomena. For the material with a cubic symmetry, elastic constants C_{11}, C_{12}, and C_{44} are sufficient to explain the whole mechanical property. Mechanical stability should be examined by the Born elastic stability criteria [112] $C_{11} > 0$, C_{11} - $C_{12} > 0$, $C_{11} + 2C_{12} > 0$, C_{44} and $C_{12} < \mathrm{B}_0 < C_{11}$. The calculated values of elestic constants are represented in table 5.2. The positive values of the constants shows the mechanical stability of the compounds under all pressure as well as in ambient condition by satisfying born stablity criteria. Cauchy pressure [113], the difference between C_{12} and C_{44} shows our system has metallic bonding under all pressure. The information about the resistance to the volume change caused by external pressure is provided by the isotropic bulk modulus. We employed Viogt-Russel-Hills approximation [114–117] which makes use of C_{11} and C_{12} elastic constants to figure out the

bulk modulus. Bulk modulus can be expressed mathmatically by the relation,

$$B = \frac{C_{11} + 2C_{12}}{3} \tag{5.1}$$

Shear modulus can be used to explain hardness and resistance to reversible deformation. It can be seen below, one can determine the shear modulus by the equation,

$$G = \frac{G_v + G_R}{2} \tag{5.2}$$

where G_R (Reuss's shear modulus) is the lower limit of G and G_v (Voight's shear modulus) is the upper limit of G and are expressed as

$$G_v = \frac{1}{5}(3C_{44} + C_{11} - C_{12}); \qquad G_v = \frac{5(C_{11} - C_{12})C_{44}}{3(C_{11} - C_{12} + 4C_{44}} \tag{5.3}$$

With Bulk and Shear modulus, Young's modulus can be calculated for the compound by the relation,

$$E = \frac{9BG}{3B + G} \tag{5.4}$$

Further the brittile and ductile nature of a compound can be understood by the Pugh's ratio (B/G) and Poisson's ratio (ν) [118] which is an important property for practical device febrication. The properties like ductility, striffness, brittileness etc are considered from Pugh's ratio and Poission's ratio. The compound with a value of B/G and ν heigher than 1.75 and 0.26 is considered to be ductile and supposed to be applicable to device febrication. But Poisson's ratio equal to 0.26 shows brittile nature and less than 0.26, the compound is considered to be plastic [119]. It is clear from table 5.1 that the values of ν and B/G for K_2SeCl_6 at ambient and under all induced pressure has a value greater than 0.26 and 1.75 respectively which pridict our studied compounds are ductile in nature and suitable for device febrication. Further Zener's anisotropy (A) [120, 121] factor can be calculated from equation 5.5 to reveal the anisotropic nature of the compounds.

$$A = \frac{2C_{44}}{C_{11} - C_{12}} \tag{5.5}$$

In summary, when K_2SeCl_6 is subjected to an external pressure, its mechanical stability increases gradually with decreased cell volume. Pugh's ratio and Poisson's ratio shows highly ductile behavior at 80 GPa with some substantial influence on the bond length. These mechanical stability permits the material to be an excillent candidate for practical applications.

5.3 Optical properties

The influence of pressure on the optical properties of a material encompasses changes in electronic transitions, alterations in lattice vibrations impacting phonon modes, variations in density affecting the refractive index, and the potential for phase transitions. To comprehend the nature of light-matter interaction of our system for practical applications, we have calculated and plotted the optical properties of K_2SeCl_6 under induced pressure in Figures 5.6 to 5.8. In this study, we elaborated the complex dielectric function $\varepsilon(\omega)$, absorption coefficient $\alpha(\omega)$, optical conductivity $\sigma(\omega)$, reflectivity $R(\omega)$, and refractive index $n(\omega)$ to illuminate band gap-dependent optical features upto 80 GPa applied pressure compared to 0 GPa. In Figure 5.6 (a), the real dielectric function of K_2SeCl_6 is depicted under all applied pressures. It's noteworthy that a material exhibiting a higher $\varepsilon_1(0)$ signifies a lower rate of charge recombination, leading to enhanced performance in optoelectronic devices [122]. Under ambient pressure, K_2SeCl_6 displays its initial peak in the visible region, which decreases with the rise in photon energy. Furthermore, K_2SeCl_6 exhibits a negative $\varepsilon_1(0)$ at an energy of 5 eV, suggesting high reflectivity at that energy, as evident in Figure 5.8 (a). For 5 GPa applied pressure, K_2SeCl_6 maintains a negative $\varepsilon_1(0)$, but with further increases in pressure, $\varepsilon_1(0)$ consistently becomes positive. At 80 GPa, the first peak shifts towards the infrared region. The second peak's value exhibits a gradual increase with induced pressure, and the magnitude of $\varepsilon_2(0)$ is closely associated with the material's band structure and density of states. For K_2SeCl_6, the threshold is at 2.502 eV, as seen in the $\varepsilon_2(\omega)$ curve, which aligns with the electronic band gap extracted from the band structure. The first peak for 0 GPa occurs in the early ultraviolet region. With applied pressure, the value of $\varepsilon_2(\omega)$ gradually

decreases, and the first peak shifts towards the ultraviolet region. Comparing to 0 GPa, the first peak of $\varepsilon_2(\omega)$ for 80 GPa is significantly smaller. However, in the range between 8 to 10 eV, $\varepsilon_2(\omega)$ increases gradually with applied pressure. For 80 GPa, $\varepsilon_2(\omega)$ reaches its maximum in this region.

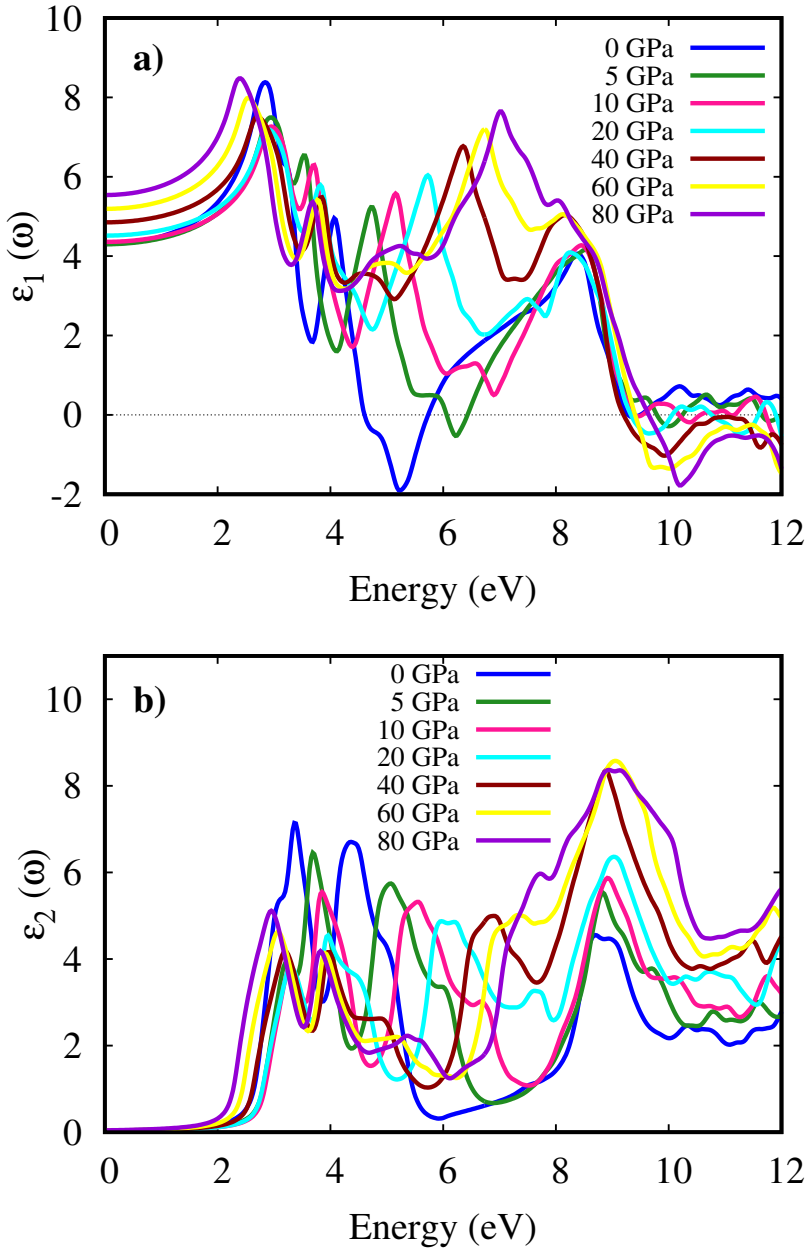

Figure 5.6: The computed a) Real dielectric function and b) Imaginary dielectric function of vacancy-ordered double perovskite K_2SeCl_6 under all applied pressure.

Beyond 10 eV, $\varepsilon_2(\omega)$ decreases with increased photon energy. This behavior aligns

with the absorption coefficient plot for the compound in Figure 5.7 (a). A material's ability to absorb electromagnetic waves provides crucial information about its efficiency in converting solar energy when exposed to sunlight.

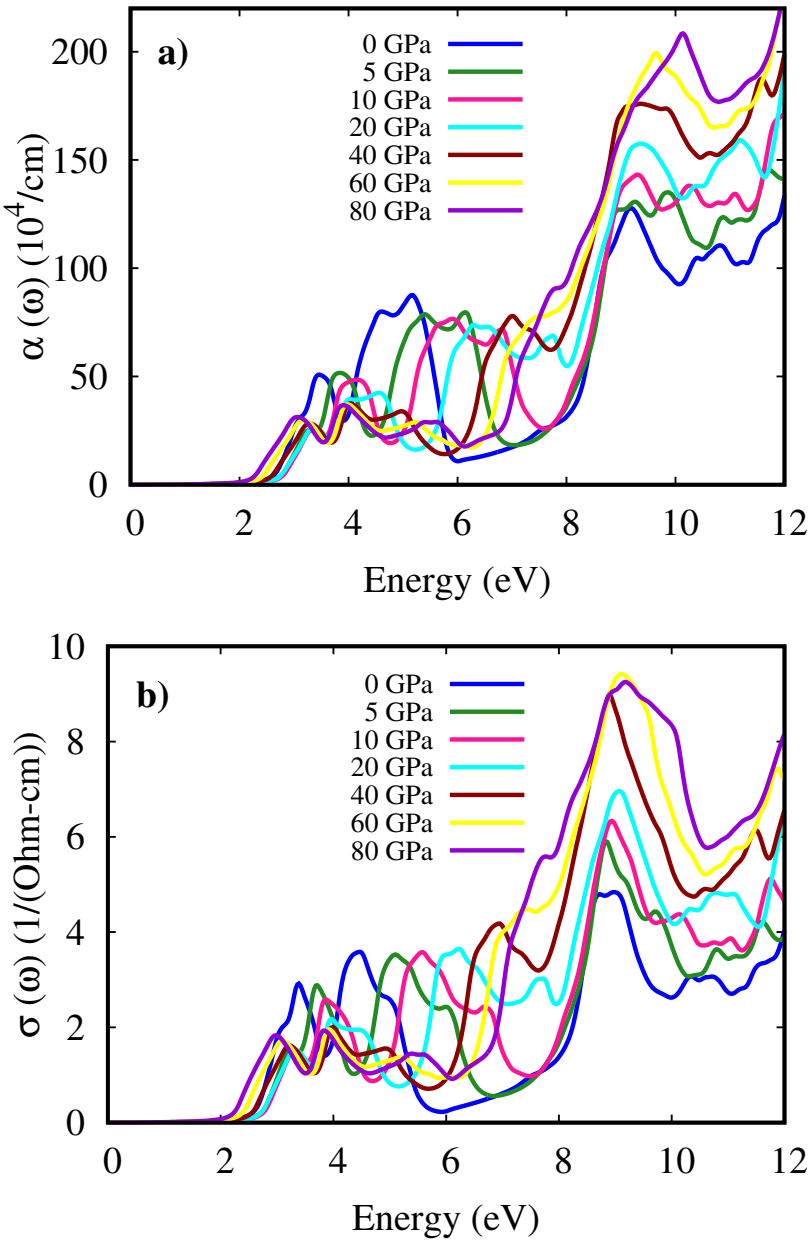

Figure 5.7: Computed a) Absorption coefficient and b) Optical conductivity of vacancy-ordered double perovskite K_2SeCl_6 under all applied pressure compared to 0 GPa.

The attenuation of light with a specific energy into a material is determined by the optical absorption coefficient α of a material [123]. Under ambient pressure, the

extracted absorption edge at 2.502 eV aligns with the electronic band gap. Beyond the threshold, as photon energy increases, $\alpha(\omega)$ reaches its first peak at 3.5 eV and the second peak at 4.5 eV. After 5 eV, the absorption coefficient starts decreasing with further increase in photon energy, revealing the semiconducting nature of the computed material.

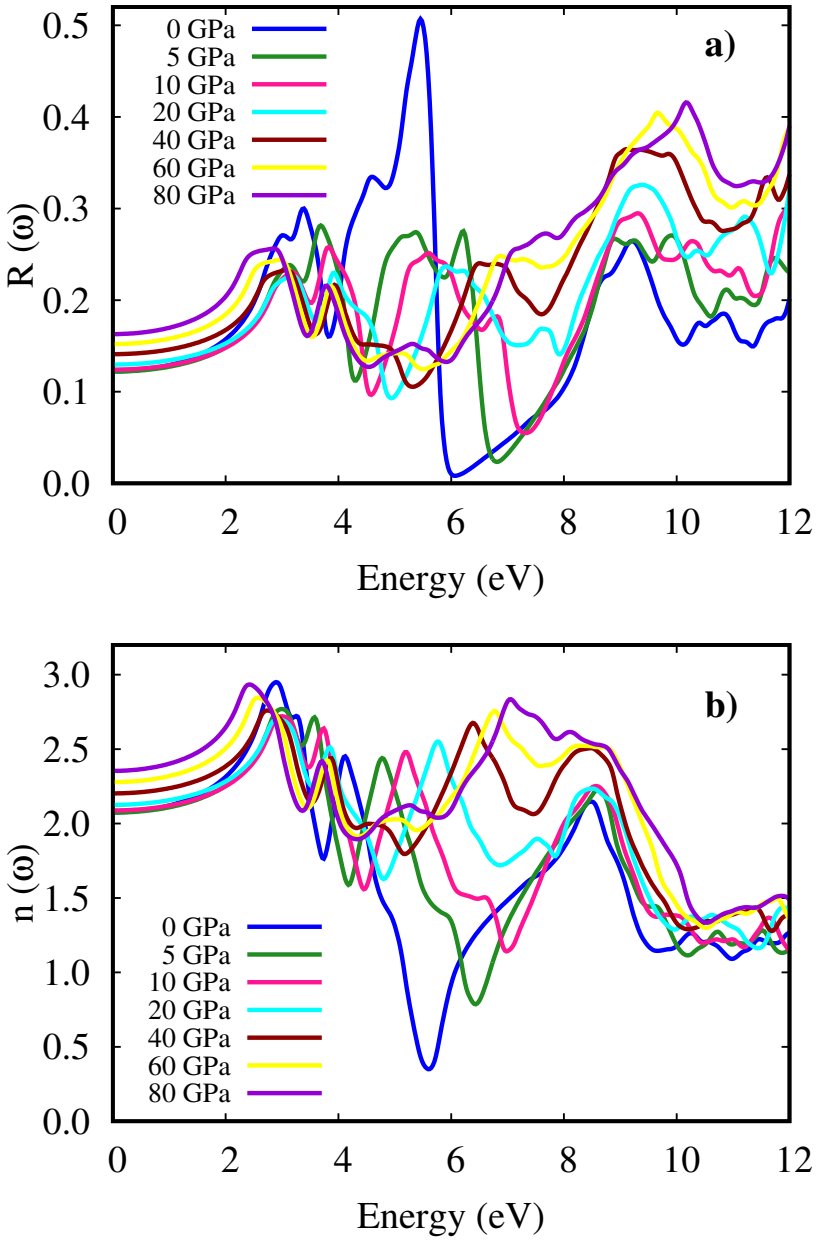

Figure 5.8: Calculated pressure induced a) Optical reflectivity and b) Refractive index of K_2SeCl_6 with ambient condition.

Under applied pressure at early UV region, value of α decreases and after 8 eV absorption increases as the photon energy increases. There is a substantial increase in absorption between the 10-12 eV region compared to 0 GPa. The electrical conductivity $\sigma(\omega)$ reflects the optical current induced by liberated free carriers resulting from incident energy. The incident photon energy excites bound valence electrons, causing them to move to the conduction band. The behavior of the absorption coefficient in Figure 5.7 (a) and optical conductivity in Figure 5.7 (b) aligns because the attenuation of incident light increases the electron concentration in the conduction band. The peaks of σ become sharper with the application of hydrostatic pressure in the UV region (at 9 eV), similar to α. This is due to the optical absorption of the studied perovskite under uniform pressure increasing between 8 to 10 eV. This result is also supported by the pressure-induced change in the band structure. Reflectivity is a crucial optical feature for materials in photovoltaic applications. For 0 GPa, reflectivity starts increasing after the threshold. The first peak occurs at the boundary of the visible spectrum and makes a sharp peak at 5 eV, where reflectivity is 50% of the incident electromagnetic wave. Under applied pressure, there is no significant change in reflectivity compared to 0 GPa. In the visible region, the maximum reflectivity is less than 30% for all applied pressures. Such a small value of R doesn't significantly impact the performance of any optical device. The refractive index $n(\omega)$ is used to determine the amount of light bent or refracted as it enters a substance. $n(\omega)$, sensitive to the wavelength, group velocity, and nature of the material, is also calculated and plotted against the photon energy in Figure 5.8 (b). Under all applied pressures compared to 0 GPa, $n(\omega)$ increases when light energy enters the UV region, and for 80 GPa, it becomes maximum (2.7). There is a significant influence of applied pressure on the refractive index over 0 GPa.

In summary, the calculated optical properties under applied pressure, compared to ambient conditions, indicate an enhanced optical usability of K_2SeCl_6 as an optoelectronic device.

5.4 Thermoelectric properties

Changes in pressure can indeed influence the thermoelectric properties of a material. The impact is material-specific, and the outcome can either enhance or diminish the material's thermoelectric performance. Increased pressure can affect electrical conductivity in diverse ways, depending on the material. It may enhance conductivity in some cases by reducing lattice defects and improving charge carrier mobility. Conversely, it might have the opposite effect by narrowing the bandgap or altering the electronic structure. For many materials, heightened pressure tends to decrease thermal conductivity by reducing phonon scattering. This reduction is advantageous for thermoelectric materials since lower thermal conductivity translates to better thermoelectric efficiency. The pressure-induced thermoelectric characteristics of K_2SeCl_6 are investigated by computing electrical conductivity (σ/τ), Seebeck coefficient (S), thermal conductivity (κ_e/τ), power factor (PF = $\sigma S^2/\tau$), and figure of merit (ZT = $\sigma S^2/\kappa\tau$). Here, τ represents the relaxation time, typically with a constant value on the order of 10^{-14}s for a semiconductor. The computed electrical conductivity per relaxation time (σ/τ) for K_2SeCl_6 under ambient and applied pressure conditions is illustrated in Figure 5.9 (a) over a temperature range from 100K to 1000K. The figure indicates that under ambient pressure, the electrical conductivity increases linearly with temperature, suggesting a rise in carrier concentration associated with electrical conduction. The continuous increase in electrical conductivity signifies a steadily growing carrier concentration, indicating a negative temperature coefficient of resistivity, which supports the semiconductor nature of the examined compound. At 100K, K_2SeCl_6 exhibits a minimum value of σ/τ, indicating suppressed charge carrier mobility, likely associated with its wide band gap. With applied pressure, the value of σ/τ continuously increases with temperature. At 80 GPa, σ/τ reaches its maximum, suggesting that with increasing pressure, more electrons get excited and contribute to the rise in carrier concentration. The thermal conductivity κ_e/τ in Figure 5.9 (b) for ambient pressure follows a similar pattern as σ/τ, resulting from the increase in temperature that enhances the kinetic energy of the carriers. For any thermoelectric material, achieving an optimized balance between electronic and thermal conductivities is crucial for higher thermoelectric efficiency.

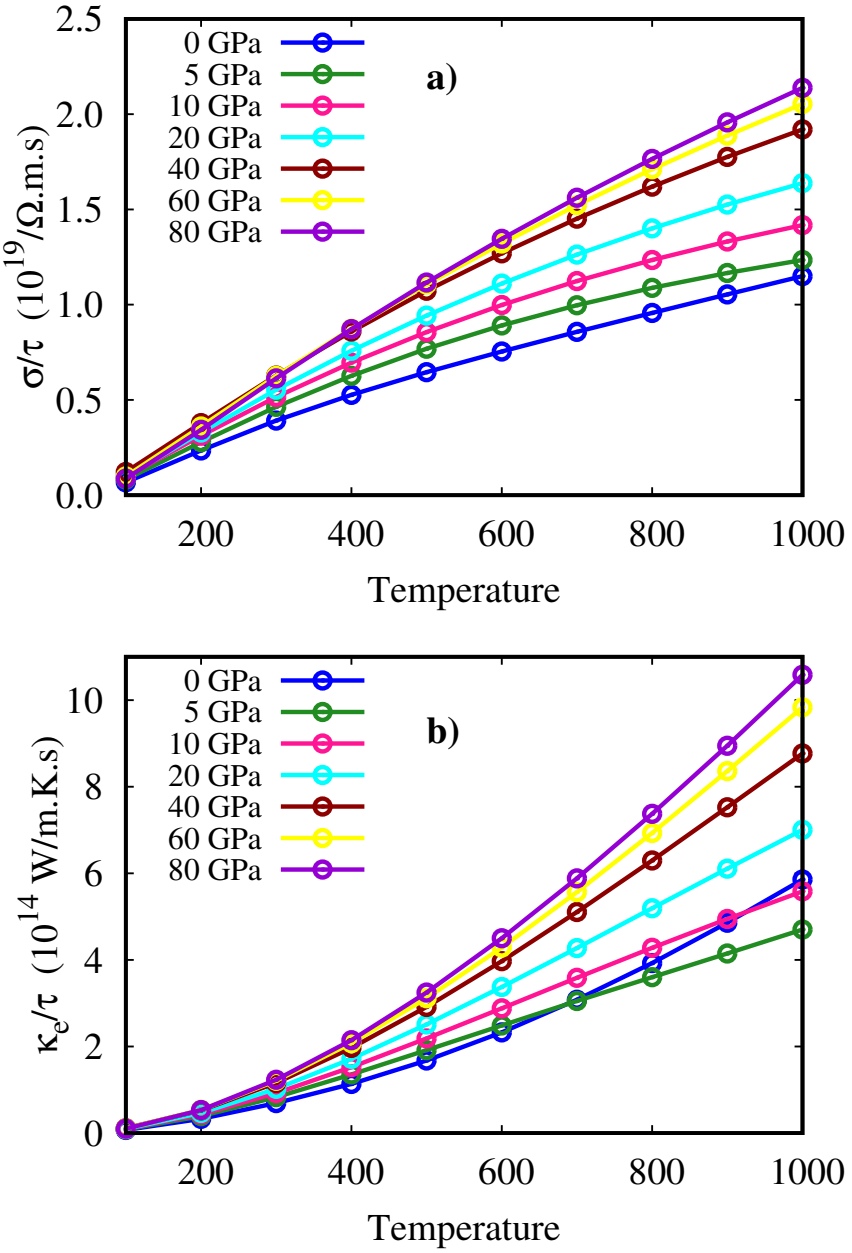

Figure 5.9: Calculated a) Electrical conductivity (σ/τ) and b) Thermal conductivity (k_e/τ) of K_2SeCl_6 under pressure as a function of temperature (T) compared to the ambient condition.

Under ambient pressure, κ_e/τ improves from 0 to 6×10^{14} W/mKs at 1000K. Following the same trend under all applied pressures, κ_e/σ continuously increases with temperature. The Seebeck coefficient quantifies how much voltage will be produced when there is a temperature difference between the two ends of a material. In simpler terms, it reflects a material's ability to convert heat energy into electric voltage.

From Figure 5.10 (a), at ambient pressure, the Seebeck coefficient decreases from 305 μV/K to 190 μV/K at 1000K temperature. The increase in σ/τ corresponds to a decrease in the potential barrier, which can potentially diminish the conversion efficiency.

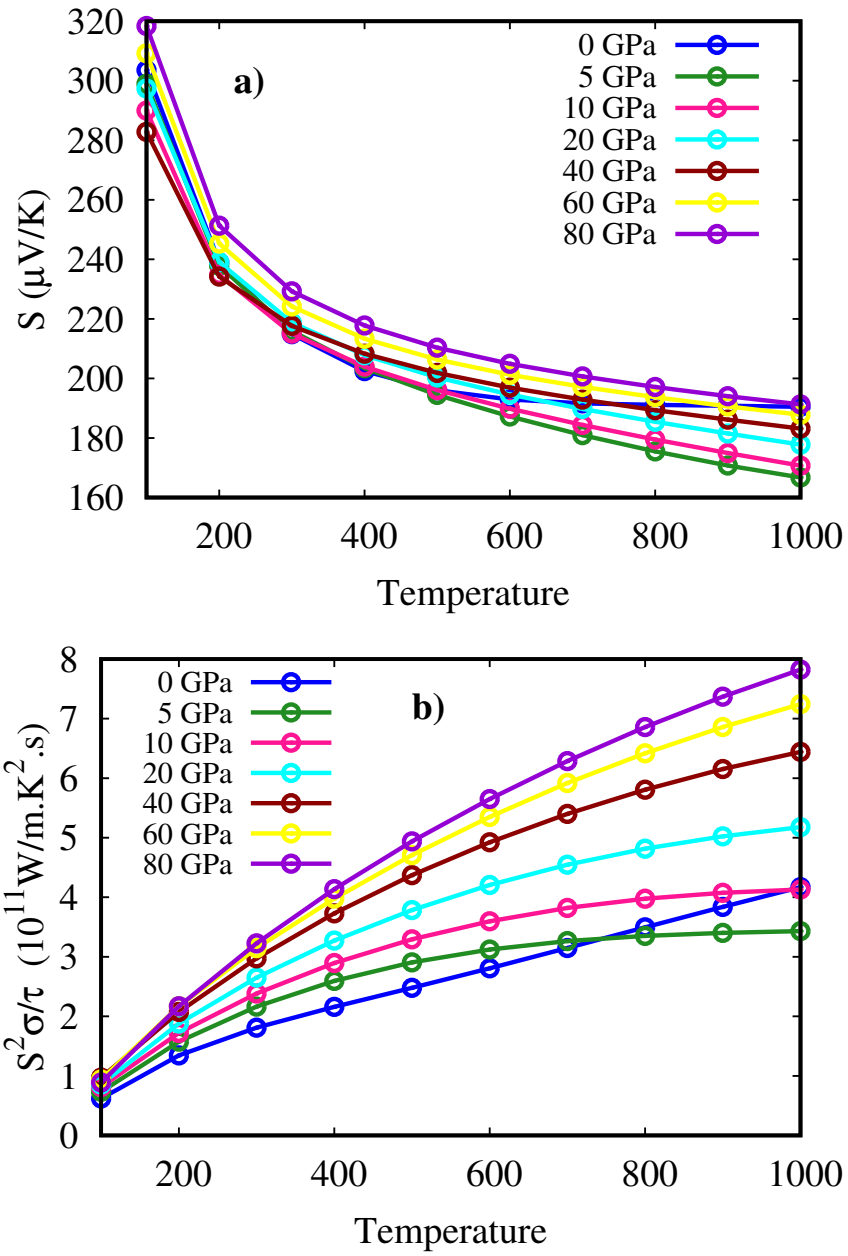

Figure 5.10: Pressure induced thermoelectric properties: a) Seebeck coefficient and b) Power factor (PF) of K_2SeCl_6 as a function of temperature (T) compared to the ambient condition.

Table 5.3: The depicted values of Electrical conductivity (σ/τ), Thermal conductivity (κ_e/τ), Seeback coefficient (S), Power factor (PF), and Figure of Merit (ZT) of K_2SeCl_6 for different pressures at 300K temperature.

Pressure (GPa)	σ/τ ($\times 10^{19}\Omega$ms)	k_e/τ ($\times 10^{14}$W/mK)	S (μV)/K	PF ($\times 10^{11}$ W/mK^{2}s)	ZT
0	0.39	0.69	214	1.80	0.784
5	0.46	0.83	215	2.16	0.780
10	0.52	0.92	215	2.38	0.775
20	0.55	1.02	218	2.64	0.777
40	0.63	1.15	218	2.97	0.770
60	0.63	1.21	224	3.14	0.781
80	0.61	1.23	229	3.22	0.786

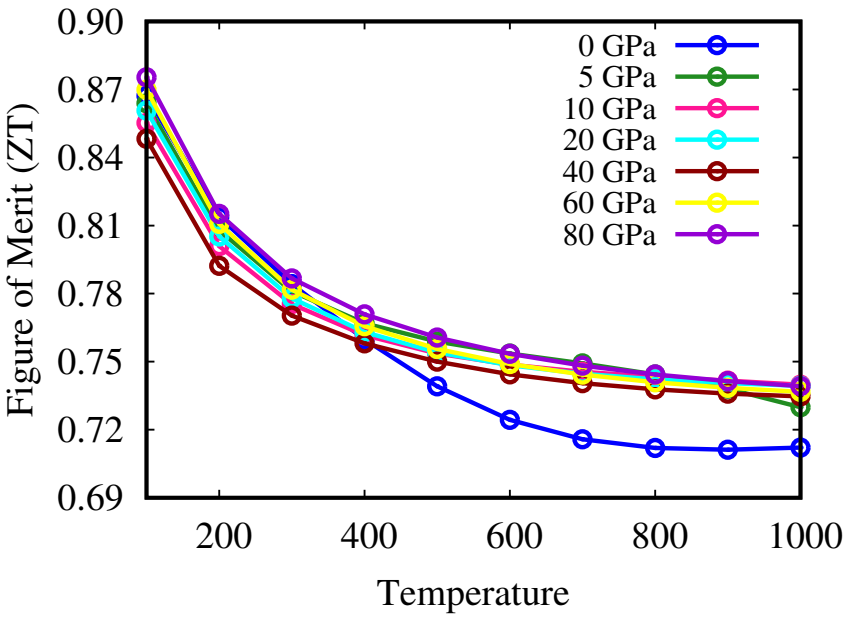

Figure 5.11: Pressure induced Figure of merit (ZT) for K_2SeCl_6 as a function of temperature (T) compared to the ambient condition.

Seebeck coefficient values exceeding 200 μV/K are considered indicative of excellent thermoelectric materials [109]. Notably, our calculations reveal a Seebeck coefficient of 214 μV/K at room temperature for K_2SeCl_6 under ambient pressure, which is remarkably outstanding to the mentioned value. Additionally, under all applied pressures, the Seebeck coefficient gradually increases compared to 0 GPa, as shown

in Table 5.3. Therefore, the studied double perovskite material exhibits excellence for thermoelectric applications under various conditions. The power factor, a dimensionless parameter characterizing the efficiency of a material in converting heat into electrical energy, is a crucial metric for assessing thermoelectric performance. A high power factor is desirable for efficient thermoelectric materials. In our system, the power factor (PF = $\sigma S^2/\tau$) demonstrates an increase from 0.6 to 4.2×10^{11} W/mK^{2}s under ambient pressure at 1000K temperature, as illustrated in Figure 5.10 (b). This trend continues with a gradual increase as pressure is applied. For a more precise assessment of thermal-to-electrical energy conversion, the figure of merit (ZT = $\sigma S^2/\kappa\tau$) is determined and plotted in Figure 5.11 for temperature ranges from 100 to 1000K. Under ambient pressure and at 100K temperature, ZT is 0.87 for K_2SeCl_6 and decreases with temperature, exhibiting 0.784 at 300K. As temperature further increases, ZT continues to decrease. With induced pressure, there are no significant changes in ZT values. The value decreases for 5, 20, and 40 GPa and reaches almost the same value for 80 GPa compared to 0 GPa.

In summary, subjecting K_2SeCl_6 to pressure increases its electrical and thermal conductivity, resulting in more free electrons in the conduction band and ensuring higher thermoelectric performance as a practical device.

Chapter 6

Conclusions

In this thesis, the physical properties of vacancy-ordered double perovskite K_2SeCl_6 were studied based on Full Potential Linear Augmented Plane Wave (FP-LAPW) method using Density Functional Theory (DFT) as implemented in WIEN2k code. We explored the structural, mechanical, electrical, optical, and thermoelectric properties of vacancy-ordered double perovskite K_2SeCl_6 for upto 80 GPa induced pressure compared to ambient condition.

The electronic bandstructure of K_2SeCl_6 revealed a p-type semiconducting nature with an indirect band gap of 2.502 eV that decreases to 1.568 eV at 80 GPa induced pressure. The top of the valence bands primarily originated from Cl 3p, while both Cl 3p and Se 4p contribute to the bottom of the conduction band for all pressurized conditions. With increasing pressure, Se 4p and Cl 3p orbitals shift from the valence region to the conduction region, contributing to a reduction in the band gap. The compound's stability and ductility under pressurized conditions are assured by its mechanical properties. The reduction in bond length and volume, combined with Pugh's and Poisson's ratios, ensure excellent stability for the compound under all pressurized conditions. Optical parameters, including dielectric constants, absorption coefficients, and optical conductivity, reveal improved optoelectronic properties in the visible and ultraviolet region under all induced pressures compared to the

ambient condition. Thermoelectric properties has been investigated using electrical conductivity, thermal conductivity, seebeck coefficient, power factor, and figure of merit. At ambient pressure, the figure of merit for K_2SeCl_6 is calculated to be 0.78, and it decreases as the temperature increases. When pressure is applied to the structure, there are no significant changes in the ZT values. However, in the high-temperature region, as the pressure increases, the value of ZT increases and reaches its maximum at 80 GPa compared to the ambient condition. That ensures the improved thermoelectric properties of our compound with induced pressure in the high-temperature region.

In summary, under pressure, the structural, mechanical, electrical, optical, and thermoelectronic properties collectively demonstrate an improved carrier concentration, coupled with good electrical and thermal conductivity, compared to ambient conditions. This suggests that the vacancy-ordered double perovskite K_2SeCl_6 under uniform pressure could be an appealing choice for applications in optoelectronics and thermoelectric power generation.

Bibliography

[1] Preeti Bhumla, Manjari Jain, Sajjan Sheoran, and Saswata Bhattacharya. Vacancy-ordered double perovskites Cs_2BI_6 (B = Pt, Pd, Te, Sn): An emerging class of thermoelectric materials. *J. Phys. Chem. Lett.*, 13:11655–11662, 12 2022.

[2] Pankaj P. Khirade and Anil V. Raut. Perovskite structured materials: Synthesis, structure, physical properties and applications. chapter 1. IntechOpen, Rijeka, 2022.

[3] Xia-Xia Ma and Ze-Sheng Li. Influence of Sn/Ge cation exchange on vacancy-ordered double perovskite $Cs_2Sn_{1-x}Ge_xI_6$: A first-principles theoretical study. *Phys. Status Solidi B Basic Res.*, 256, 11 2018.

[4] Muhammad Usman and Qingfeng Yan. Recent advancements in crystalline Pb Free halide double perovskites. *CRYS.*, 10(2), 2020.

[5] Sami Vasala and Maarit Karppinen. $A_2BB'O_6$ perovskites: A review. *Prog. Solid. State Ch.*, 43(1):1–36, 2015.

[6] S. Mohanty and S Behera. Multifunctional properties of transition metal based double perovskite ceramics. *Chem. Phys. Impact.*, 7:100259.

[7] $A_2BB'O_6$ perovskites: A review. *Prog. Solid. State Ch.*, 43(1):1–36, 2015.

[8] Massimiliano Cavallini and Denis Gentili. Atomic vacancies in transition metal dichalcogenides: Properties, fabrication, and limits. *ChemPlusChem*, 87(3):e202100562, 2022.

[9] S. Mohanty and S Behera. Multifunctional properties of transition metal based double perovskite ceramics. *Chem. Phys. Impact.*, 7:100259, 2023.

[10] S. Mishra and S.K. Parida. Electrical and optical properties of a lead-free complex double perovskite $BaNaFeMoO_6$: Photovoltaic and thermistor applications. *J. mater. sci. eng., B*, 296:116629, 2023.

[11] Sebastián Larrégola, José Alonso, Denis Sheptyakov, Miguel Algueró, Angel Muñoz, Vladimir Pomjakushin, and José Pedregosa. An original polymorph sequence in the high-temperature evolution of the perovskite Pb_2TmSbO_6. pages 14470–80, 10 2010.

[12] Synthetic approaches for perovskite thin films and single-crystals. *Energy Advances*, 2(8):1075–1115, 2023.

[13] Muhammad Faizan, Guoqi Zhao, Tianxu Zhang, Xiaoyu Wang, Xin He, and Lijun Zhang. Elastic and thermoelectric properties of vacancy ordered double perovskites A_2BX_6: A DFT study. *Acta Phys. Chim*, page 2303004, 01 2023.

[14] Annalise Maughan, Alex Ganose, David Scanlon, and James Neilson. Perspectives and design principles of vacancy-ordered double perovskite halide semiconductors. *Chem. Mater.*, 31, 01 2019.

[15] Preeti Bhumla, Manjari Jain, Sajjan Sheoran, and Saswata Bhattacharya. Vacancy-ordered double perovskites A_2BX_6 (A = Cs, B = Pt, Pd, Te, Sn, X = I): An emerging class of thermoelectric materials, 09 2022.

[16] Aslam Hossain, Sanjay Roy, and K. Sakthipandi. The external and internal influences on the tuning of the properties of perovskites: An overview. *Ceram. Int.*, 45(4):4152–4166, 2019.

[17] Ankur Yadav, Farha Mansoorie, Ankush Saini, and M. Bag. Vacancy ordered lead free double perovskite based flexible supercapacitor for sustainable energy applications. *ACS Sustain. Chem. Eng.*, 12, 01 2024.

[18] Shammya Afroze, AfizulHakem Karim, Quentin Cheok, Sten Eriksson, and Abul Azad. Latest development of double perovskite electrode materials for solid oxide fuel cells: a review. *Front. Energy*, 13, 11 2019.

[19] Xian-Hao Zhao, Xiao-Nan Wei, Tian-Yu Tang, Quan Xie, Li-Ke Gao, Li-Min Lu, De-Yuan Hu, Li Li, and Yan-Lin Tang. Theoretical prediction of the structural, electronic and optical properties of vacancy-ordered double perovskites Tl_2TiX_6 (X = Cl, Br, I). *J. Solid State Chem.*, 305:122684, 2022.

[20] Annalise Maughan, Alex Ganose, David Scanlon, and James Neilson. Perspectives and design principles of vacancy-ordered double perovskite halide semiconductors. *Chem. Mater.*, 31, 01 2019.

[21] George Njema and Joshua Kibet. A review of the technological advances in the design of highly efficient perovskite solar cells. *Int. J. Photoenergy .*, 2023:1–35, 08 2023.

[22] Yingzhi Zhou, Jing Wang, Dongxiang Luo, Dehua Hu, Yonggang Min, and Xue Qifan. Recent progress of halide perovskites for thermoelectric application. *Nano Energy*, 94:106949, 01 2022.

[23] Advancements and challenges in molecular/hybrid perovskites for piezoelectric nanogenerator application: A comprehensive review. *Nano Energy*, 120:109101, 2024.

[24] Md Azimul Haque, Mohamad Nugraha, Sri Harish Kumar Paleti, and Derya Baran. Role of compositional tuning on thermoelectric parameters of hybrid halide perovskites. *J. Phys. Chem. C*, 05 2019.

[25] Aiyeshah Alhodaib. Study of vacancy ordered double perovskites In_2PtX_6 (X = Cl, Br, I) for solar cells and renewable energy, alternative of hybrid perovskites. *J. Solid State Chem.*, 309:123015, 2022.

[26] Fei Zhang, Zhipeng Chen, Zibin Liu, Mochen Jia, Xu Chen, Di Wu, Xinjian Li, and Zhifeng Shi. Highly stable vacancy-ordered double perovskite Rb_2ZrCl_6

with broadband emission for down-conversion white light-emitting diodes. *J. Lumin.*, 251:119150, 2022.

[27] Muhammad Faizan, Dr Bhamu, Ghulam Murtaza, Xin He, Neeraj Kulhari, Murefah AL-Anazy, and Shah Khan. Electronic and optical properties of vacancy ordered double perovskites A_2BX_6 (A = Rb, Cs; B = Sn, Pd, Pt; and X = Cl, Br, I): a first principles study. *Sci. Rep.*, 11:6965, 03 2021.

[28] B. Cucco, G. Bouder, L. Pedesseau, C. Katan, J. Even, M. Kepenekian, and G. Volonakis. Electronic structure and stability of Cs_2TiX_6 and Cs_2ZrX_6 (X = Br, I) vacancy ordered double perovskites. *Appl. Phys. Lett.*, 119(18):181903, 11 2021.

[29] Preeti Bhumla, Manjari Jain, Sajjan Sheoran, and Saswata Bhattacharya. Vacancy-ordered double perovskites Cs_2BI_6 (B = Pt, Pd, Te, Sn): An emerging class of thermoelectric materials. *J. Phys. Chem. Lett.*, 13(50):11655–11662, 2022. PMID: 36503226.

[30] Jiahao Li, Liping Sun, Xiuhong Cao, and Jing Chang. First-principles predictions of structural, mechanical, and optoelectronic properties of Se-based double perovskites A_2SeX_6 (A = Rb, K; X = Cl, Br, I). *J. Phys. Chem. C*, 127(21):10332–10340, 2023.

[31] Paul Bingham, Andrew Connelly, N. Cassingham, and N. Hyatt. Oxidation state and local environment of selenium in alkali borosilicate glasses for radioactive waste immobilisation. *J Non Cryst Solids.*, 357:2726–2734, 07 2011.

[32] Ismahan Duz Parrey, Fuat Bilican, Celal Kursun, Hasan Huseyin Kart, and Khursheed Ahmad Parrey. Mechanical stability and energy gap evolution in Cs-Based Ag, Bi halide double perovskites under high pressure: A theoretical DFT approach. *ACS Omega*, 8(29):26577–26589, 2023.

[33] Annalise Maughan, Alex Ganose, David Scanlon, and James Neilson. Perspectives and design principles of vacancy ordered double perovskite halide semiconductors. *Chem. Mater.*, 31, 01 2019.

[34] M.A. Ghebouli, T. Chihi, B. Ghebouli, and M. Fatmi. Study of the structural, elastic, electronic and optical properties of lead free halide double perovskites Cs_2AgBiX_6(X= Br, Cl). *Chin. J. Phys.*, 56(1):323–330, 2018.

[35] Eric Yang and Xuan Luo. Theoretical pressure-tuning bandgaps of double perovskites $A_2(BB')X_6$ for photo-voltaics. *Sol. Energy*, 207:165–172, 09 2020.

[36] Francisco Javier Manjon and Daniel Errandonea. Pressure-induced structural phase transitions in materials and earth sciences. *Phys. Status Solidi B Basic Res.*, 246:9 – 31, 01 2009.

[37] John S Tse. A chemical perspective on high pressure crystal structures and properties. *Natl. Sci.*, 7(1):149–169, 10 2019.

[38] Mohammed Miri, Younes Ziat, Hamza Belkhanchi, Zakaryaa Zarhri, and Youssef Ait El Kadi. Structural and optoelectronic properties of LiYP (Y = Ca, Mg, and Zn) half-heusler alloy under pressure: A DFT study. *Phys. B: Condens.*, 667:415216, 2023.

[39] Enlai Dong, Bo Liu, Qing Dong, Xuhan Shi, Xin Ma, Ran Liu, Xuebin Zhu, Xuan Luo, Xiaodong Li, Yanchun Li, Quanjun Li, and Bingbing Liu. Effects of pressure on the structure and properties of layered ferromagnetic $Cr_2Ge_2Te_6$. *Phys. B: Condens.*, 595:412344, 2020.

[40] Nazila Zarabinia and Reza Rasuli. Electronic and optical properties of halide double-perovskites under strain: a density functional study. *Energy Sources A: Recovery Util. Environ.*, 43:1–13, 01 2021.

[41] Z. Arnold, O. Isnard, H. Mayot, M. Míšek, and J. Kamarád. Pressure effect on magnetic properties of $RCo_{12}B_6$ (R=Y, Ce) compounds. *J. Magn. Magn. Mater.*, 322(9):1117–1119, 2010. Proceedings of the Joint European Magnetic Symposia.

[42] I.S Dubenko, I.Yu Gaidukova, Y Hosokoshi, K Inoue, and A.S Markosyan. Concentration and pressure dependence of magnetic ordering in

$Y(Mn_{1-x}Me_x)_2$ compounds with Me=Al, Fe and Ni. *J. Magn. Magn. Mater.*, 195(3):687–691, 1999.

[43] Pierre Hohenberg and Walter Kohn. Inhomogeneous electron gas. *Phy. Rev.*, 136(3B):B864, 1964.

[44] Kieron Burke. Perspective on density functional theory. *Chem. Phys.*, 136:150901, 04 2012.

[45] P. Blaha, Karlheinz Schwarz, P. Sorantin, and S.B. Trickey. Blaha, p., Schwarz, K., Sorantin, p. and Trickey, s.b. full-potential, linearized augmented plane wave programs for crystalline systems. comput. phys. commun. 59, 399-415. *Comput. Phys. Commun.*, 59:399–415, 06 1990.

[46] Peter Blaha, Karlheinz Schwarz, Fabien Tran, Robert Laskowski, Georg K. H. Madsen, and Laurence D. Marks. WIEN2k: An APW+lo program for calculating the properties of solids. *Chem. Phys.*, 152(7):074101, 02 2020.

[47] Chapter 11 - ELECTRONIC MOTION: DENSITY FUNCTIONAL THEORY (DFT). pages 567–614. Elsevier, Amsterdam, 2007.

[48] Philip J. Hasnip, Keith Refson, Matt I. J. Probert, Jonathan R. Yates, Stewart J. Clark, and Chris J. Pickard. Density functional theory in the solid state. *Philos. Trans.*, 372(2011):20130270, 2014.

[49] Peter Blaha, Karlheinz Schwarz, Fabien Tran, Robert Laskowski, Georg Madsen, and Laurence Marks. WIEN2k: An APW+lo program for calculating the properties of solids. *Chem. Phys.*, 152:074101, 02 2020.

[50] Stefan Blügel and Gustav Bihlmayer. Full-potential linearized augmented planewave method. *J Comput Theor Nanosci.*, 31:85–129, 2006.

[51] Georg Madsen and David Singh. BoltzTraP. a code for calculating band-structure dependent quantities. *Comput. Phys. Commun.*, 175:67–71, 07 2006.

[52] G Robert. Parr and weitao yang, density functional theory of atoms and molecules, 1989.

[53] Max Born. On the quantum mechanics of collision processes. 2021:0828, 09 2021.

[54] Nouredine Zettili. Quantum mechanics: concepts and applications, 2003.

[55] G Robert. Parr and weitao yang, density functional theory of atoms and molecules, 1989.

[56] Michael P Marder. *Condensed matter physics*. John Wiley & Sons, 2010.

[57] David J Griffiths and Darrell F Schroeter. *Introduction to quantum mechanics*. Cambridge university press, 2018.

[58] Max Born. *Physik im Wandel meiner Zeit*. Springer Sci. Rev., 2013.

[59] Hubert Klar. The born-oppenheimer approximation revisited. *Journal of Applied Mathematics and Physics*, 8(8):1507–1514, 2020.

[60] Klaus Capelle. A bird's-eye view of density-functional theory. *Braz. J. Phys.*, 36:1318–1343, 2006.

[61] Franz Schwabl. *Quantenmechanik (QM I): Eine Einführung*. Springer Sci. Rev., 2007.

[62] Paul Adrien Maurice Dirac. A new notation for quantum mechanics. In *Mathematical Proceedings of the Cambridge Philosophical Society*, volume 35, pages 416–418. CUP, 1939.

[63] David J Griffiths and Darrell F Schroeter. *Introduction to quantum mechanics*. CUP, 2018.

[64] Christian B Lang and Norbert Pucker. *Mathematische methoden in der physik*, volume 2. Springer, 2005.

[65] A chemist's guide to density functional theory by wolfram koch (german chemical society, frankfurt am main) and max c. holthausen (Humbolt University Berlin).

[66] Attila Szabo and Neil S Ostlund. *Modern quantum chemistry: introduction to advanced electronic structure theory*. Courier Corporation, 2012.

[67] A chemist's guide to density functional theory by wolfram koch (german chemical society, frankfurt am main) and max c. holthausen (Humbolt University Berlin).

[68] Attila Szabo and Neil S Ostlund. *Modern quantum chemistry: introduction to advanced electronic structure theory*. Courier Corporation, 2012.

[69] Walter Kohn. Nobel lecture: Electronic structure of matter—wave functions and density functionals. *Rev. Mod. Phys.*, 71(5):1253, 1999.

[70] Per-Olov Löwdin. Scaling problem, virial theorem, and connected relations in quantum mechanics. *J. Mol. Spectrosc.*, 3(1):46–66, 1959.

[71] Björn O Roos. *Lecture notes in quantum chemistry*, volume 58. Springer, 1992.

[72] G Robert. Parr and weitao yang, density functional theory of atoms and molecules, 1989.

[73] Michael P Marder. *Condensed matter physics*. John Wiley & Sons, 2010.

[74] Mathieu Lewin, Elliott H Lieb, and Robert Seiringer. The local density approximation in density functional theory. *Pure Appl.*, 2(1):35–73, 2019.

[75] P. Hohenberg and W. Kohn. Inhomogeneous Electron Gas. *Phys. Rev.*, 136:B864–B871, 1964.

[76] Vikram Gavini, Kaushik Bhattacharya, and Michael Ortiz. Quasi-continuum orbital-free density-functional theory: A route to multi-million atom non-periodic dft calculation. *J Mech Phys Solids* ., 55(4):697–718, 2007.

[77] Eugene S Kryachko and Eduardo V Ludeña. *Energy density functional theory of many-electron systems*, volume 4. Springer Science & Business Media, 2012.

[78] John P Perdew. Generalized gradient approximations for exchange and correlation: A look backward and forward. *Phys. B: Condens.*, 172(1-2):1–6, 1991.

[79] Axel D Becke. Density-functional exchange-energy approximation with correct asymptotic behavior. *Phy. Rev.*, 38(6):3098, 1988.

[80] John P Perdew, JA Chevary, SH Vosko, Koblar A Jackson, Mark R Pederson, DJ Singh, and Carlos Fiolhais. Atoms, molecules, solids, and surfaces: Applications of the generalized gradient approximation for exchange and correlation. *Phy. Rev. B*, 48(7):4978, 1993.

[81] John P Perdew, K Burke, and M Ernzerhof. Perdew, burke, and ernzerhof reply. *Phys. Rev. Lett.*, 80(4):891, 1998.

[82] Ulf Von Barth and Lars Hedin. A local exchange-correlation potential for the spin polarized case. i. *J. Phys. C: Solid State Phys.*, 5(13):1629, 1972.

[83] John Perdew, Jianmin Tao, Viktor Staroverov, and Gustavo Scuseria. Meta-generalized gradient approximation: Explanation of a realistic nonempirical density functional. *Chem. Phys.*, 120:6898–911, 05 2004.

[84] Yan Zhao and Donald Truhlar. *Theor. Chem. Acc.*, 120:215–241, 04 2008.

[85] Jianwei Sun, Adrienn Ruzsinszky, and John Perdew. Scan: Strongly constrained and appropriately normed semilocal density functional. *Phys. Rev. Lett.*, 115, 04 2015.

[86] Vladimir I Anisimov, Ferdi Aryasetiawan, and AI Lichtenstein. First-principles calculations of the electronic structure and spectra of strongly correlated systems: the LDA+ U method. *J. Condens. Matter Phys.*, 9(4):767, 1997.

[87] MT Czyżyk and GA Sawatzky. Local-density functional and on-site correlations: The electronic structure of La_2CuO_6 and $LaCuO_6$. *Phy. Rev. B*, 49(20):14211, 1994.

[88] Vlasdimir I Anisimov, IV Solovyev, MA Korotin, MT Czyżyk, and GA Sawatzky. Density-functional theory and nio photoemission spectra. *Phy. Rev. B*, 48(23):16929, 1993.

[89] Erik R Ylvisaker, Warren E Pickett, and Klaus Koepernik. Anisotropy and magnetism in the LSDA+ U method. *Phy. Rev. B*, 79(3):035103, 2009.

[90] Nirpendra Singh, Dalaver Anjum, Gobind Das, Issam Qattan, Shashikant Patole, and Muhammad Sajjad. Phonon dynamics and transport properties of copper thiocyanate and copper selenocyanate pseudohalides. *ACS omega*, 5(44):28637–28642, 2020.

[91] Andreas Kaltzoglou, Maria Antoniadou, Athanassios Kontos, Constantinos Stoumpos, Dorothea Perganti, Eirini Siranidi, Vasilios Raptis, Kalliopi Trohidou, Vassilis Psycharis, Mercouri Kanatzidis, and Polycarpos Falaras. Optical-vibrational properties of the Cs_2SnX_6 (X = Cl, Br, I) defect perovskites and hole-transport efficiency in dye-sensitized solar cells. *J. Phys. Chem. C*, 120, 05 2016.

[92] Jiahao Li, Liping Sun, Xiuhong Cao, and Jing Chang. First-principles predictions of structural, mechanical, and optoelectronic properties of Se-based double perovskites A_2SeX_6 (A = Rb, K; X = Cl, Br, I). *J. Phys. Chem*, 127(21):10332–10340, 2023.

[93] Q Mahmood, Ghulam M Mustafa, Manal Morsi, Hind Albalawi, Tahani H Flemban, M Hassan, Hind Althib, M I Khan, and T Ghrib. Theoretical investigations of optoelectronic and thermoelectric properties of halide based double perovskite halides: K_2TeX_6. *Phys. Scr.*, 96(7):075703, may 2021.

[94] V. M. Goldschmidt. Die gesetze der krystallochemie. *DSci. Nat.*, 14(21):477–485, may 1926.

[95] Zhi-jian Wu, Er-jun Zhao, Hong-ping Xiang, Xian-feng Hao, Xiao-juan Liu, and Jian Meng. Crystal structures and elastic properties of superhard IrN_2 and IrN_3 from first principles. *Phys. Rev. B*, 76:054115, Aug 2007.

[96] Akihiko Yoshikawa, Hiroyuki Matsunami, and Yasushi Nanishi. *Development and Applications of Wide Bandgap Semiconductors*, pages 1–24. Springer Berlin Heidelberg, Berlin, Heidelberg, 2007.

[97] Zewen Xiao, Hechang Lei, Xiao Zhang, Yuanyuan Zhou, Hideo Hosono, and Toshio Kamiya. Ligand-hole in $[SnI_6]$ unit and origin of band gap in photovoltaic perovskite variant Cs_2SnI_6. *BCSJ*, 88(9):1250–1255, 2015.

[98] Sandeep Hnamte, Lalhriatpuia and, Himanshu Joshi, and R. Thapa. Electronic and optical properties of double perovskite Ba_2VMoO_6: FP-LAPW study. volume 1953, page 140132, 05 2018.

[99] Yao Cai, Wei Xie, Yt Teng, Harikesh P C, Biplab Ghosh, Patrick Huck, Kristin Persson, Nripan Mathews, Subodh Mhaisalkar, Matthew Sherburne, and Mark Asta. High-throughput computational study of halide double perovskite inorganic compounds. *Chem. Mater.*, 31, 07 2019.

[100] David R. Penn. Wave-number-dependent dielectric function of semiconductors. *Phys. Rev.*, 128:2093–2097, Dec 1962.

[101] P Blaha, K Schwarz, GKH Madsen, D Kvasnicka, and J Luitz. Wien2k, an augmented plane wave plus local orbitals program for calculating crystal properties, ; vienna university of technology: Vienna, austria, 2001. 2002.

[102] Qasim Mahmood, Taher Ghrib, Amani Rached, Amel Laref, and M.A. Kamran. Probing of mechanical, optical and thermoelectric characteristics of double perovskites Cs_2GeCl/Br_6 by DFT method. *Mater. Sci. Semicond.*, 112:105009, 06 2020.

[103] Jiban Kangsabanik, Vipinraj Sugathan, Anuradha Yadav, Aswani Yella, and Aftab Alam. Double perovskites overtaking the single perovskites: A set of new solar harvesting materials with much higher stability and efficiency. *Phys. Rev. Mater.*, 2:055401, May 2018.

[104] Diwen Liu, Wenying Zha, Rusheng Yuan, Benyong Lou, and Rongjian Sa. Indirect to direct band gap transition and optical properties of metal alloys of $Cs_2Te_{1-x}Ti_xI_6$: a theoretical study. *RSC Adv.*, 10:36734–36740, 2020.

[105] Oded Rabina, Yu-Ming Lin, and Mildred Dresselhaus. Anomalously high thermoelectric figure of merit in $Bi_{1-x}Sb_x$ nanowires by carrier pocket alignment. *Appl. Phys. Lett.*, 79:81–83, 07 2001.

[106] A. Shankar, D.P. Rai, Sandeep Chettri, R. Khenata, and R.K. Thapa. Fp-lapw calculations of the elastic, electronic and thermoelectric properties of the filled skutterudite $CeRu_4Sb_{12}$. *J. Solid State Chem.*, 240:126–132, 2016.

[107] Chong Xiao, Zhou Li, Kun Li, Pengcheng Huang, and Yi Xie. Decoupling interrelated parameters for designing high performance thermoelectric materials. *Acc. Chem. Res.*, 47(4):1287–1295, 2014. PMID: 24517646.

[108] Gang Zhou and Dong Wang. Few-quintuple Bi_2Te_3 nanofilms as potential thermoelectric materials. *Sci. Rep.*, 5(1):8099, 2015.

[109] Thi Kim Phuong Luong, Vinh Le Thanh, Abdelhamid Ghrib, Moustafa El Kurdi, and Philippe Boucaud. Making germanium, an indirect band gap semiconductor, suitable for light-emitting devices*. *ANSN*, 6(1):015013, jan 2015.

[110] Adam Jaffe, Yu Lin, Wendy Mao, and Hemamala Karunadasa. Pressure-induced metallization of the halide perovskite $(CH_3NH_3)PbI_3$. *J. Am. Chem. Soc.*, 139, 03 2017.

[111] Syed Gillani, Riaz Ahmad, I. Zeba, Islah Islah-u din, M. Shakil, Muhammad Rizwan, Muhammad Rafique, Muhammad Sarfraz, and S.S. Hassan. Effect of external pressure on the structural stability, electronic structure, band gap engineering and optical properties of $LiNbO_3$: An ab-initio calculation. *Mater. Today Commun.*, 23:100919, 06 2020.

[112] Félix Mouhat and François-Xavier Coudert. Necessary and sufficient elastic stability conditions in various crystal systems. *Phys. Rev. B*, 90:224104, Dec 2014.

[113] Mark E. Eberhart and Travis E. Jones. Cauchy pressure and the generalized bonding model for nonmagnetic bcc transition metals. *Phys. Rev. B*, 86:134106, Oct 2012.

[114] JAD Matthew. Dynamical theory of crystal lattices by m. born and k. huang. *Acta Cryst. A."*, 26(6):702–702, 1970.

[115] WJTL Voight. Lehrbuch der kristallphysik. *Teubner, Leipzig*, 1928.

[116] AJZAMM Reuss. Calculation of the flow limits of mixed crystals on the basis of the plasticity of monocrystals. *Z. Angew. Math. Mech*, 9:49–58, 1929.

[117] R Hill. Proc. phys. soc., london. *Sect. A*, 65:349, 1952.

[118] S.F. Pugh. Xcii. relations between the elastic moduli and the plastic properties of polycrystalline pure metals. *Lond. Edinb. Dublin philos. mag.*, 45(367):823–843, 1954.

[119] K Haddadi, A Bouhemadou, L Louail, and Y Medkour. Structural, elastic and electronic properties of $XNCa_3$ (X= Ge, Sn and Pb) compounds. *Solid State Commun.*, 149(15-16):619–624, 2009.

[120] Christopher M Kube. Elastic anisotropy of crystals. *AIP Adv.*, 6(9):095209, 2016.

[121] C Zener. Elasticity and anelasticity of metals (u. of chicago press, chicago) google scholar zener c. 1954. *Elasticity and Anelasticity of Metals*, 1948.

[122] Md Rahaman and A.K.M. Hossain. Effect of metal doping on the visible light absorption, electronic structure and mechanical properties of non-toxic metal halide $CsGeCl_3$. *RSC Adv.*, 8:33010–33018, 09 2018.

[123] Md. Arif Islam, Jakiul Islam, Md Nazrul Islam, Sapan Sen, and A.K.M. Hossain. Enhanced ductility and optoelectronic properties of environment-friendly $CsGeCl_3$ under pressure. *AIP Adv.*, 11:45014, 04 2021.